Geochimica et Cosmochimica Acta 370 (2024) 144–160

Contents lists available at ScienceDirect

Geochimica et Cosmochimica Acta

journal homepage: www.elsevier.com/locate/gca

Surface ocean biogeochemistry and deep ocean circulation control relationships between nutrient-type trace metals (Cd, Ni, Cu, and Zn) and nutrients in the South Atlantic Ocean near the subtropical front

Xue-Gang Chen [a,b], Martha Gledhill [b], Maeve C. Lohan [c], Angela Milne [d], Eric P. Achterberg [b,*]

[a] Ocean College, Zhejiang University, Zhoushan, China
[b] GEOMAR Helmholtz Centre for Ocean Research Kiel, Kiel, Germany
[c] Ocean and Earth Sciences, National Oceanography Centre, University of Southampton, Southampton, UK
[d] School of Geography, Earth and Environmental Sciences, University of Plymouth, Plymouth, UK

ARTICLE INFO

Associate editor: Tristan J Horner

Keywords:
Trace metals
Primary productivity
Water mass mixing
Southern Ocean
GEOTRACES

ABSTRACT

The ocean region along the latitude of 40°S in the South Atlantic, characterized by enhanced primary productivity, forms a transition zone between the nutrient replete but iron depleted Southern Ocean, and the nitrate and iron depleted Subtropical Gyre. Here, we present distributions of nutrient-type dissolved and particulate trace metals (dTMs and pTMs) including cadmium (Cd), nickel (Ni), copper (Cu), and zinc (Zn) in the South Atlantic from the GEOTRACES GA10 cruises. Phytoplankton uptake, riverine and atmospheric inputs shaped dTM and pTM concentrations in surface waters (dCd 27.8 ± 36.0 pmol kg^{-1}, n = 222; dCu 0.732 ± 0.429 nmol kg^{-1}, n = 222; dNi 3.38 ± 0.52 nmol kg^{-1}, n = 219; dZn 0.332 ± 0.398 nmol kg^{-1}, n = 214). Subsurface nutrients and dTMs (dCd 563 ± 184 pmol kg^{-1}, n = 335; dCu 1.819 ± 0.773 nmol kg^{-1}, n = 334; dNi 6.19 ± 1.06 nmol kg^{-1}, n = 330; dZn 3.71 ± 2.10 nmol kg^{-1}, n = 333) were controlled by the mixing of Antarctic origin waters and North Atlantic Deep Waters (NADW) with negligible contributions from local remineralization. Dissolved and particulate TMs in the Argentine Basin showed elevated concentrations towards the seafloor because of benthic inputs. Direct hydrothermal inputs of dTMs and pTMs to deep waters were not observed along the transect. The Cd-Cu-Zn-phosphate stoichiometries of Antarctic origin waters were set by a combination of dynamic physical circulation and preferential uptake of Cd, Cu, and Zn relative to phosphate in surface waters because of a dominance by diatoms in the Southern Ocean. Water mass mixing subsequently produced convoluted dCu-P and dZn-P relationships and apparent linear dCd-P and dNi-P relationships in the South Atlantic. More importantly, endmember characteristics of Antarctic waters and NADW are largely fixed in their formation regions in high latitude oceans. Therefore, the highly dynamic high latitude oceans are key regions that supply nutrients and TMs at specific ratios to low latitude oceans via the thermohaline circulation. Changes to processes in the high latitude oceans may have consequences for marine primary productivity downstream, and hence the global carbon cycle.

1. Introduction

Cadmium (Cd), copper (Cu), nickel (Ni), and zinc (Zn) are essential micronutrients for phytoplankton growth and functioning in the ocean (Bruland et al., 2014; Morel and Price, 2003). Dissolved (filter pore size < 0.2 μm) Cd (dCd), Cu (dCu), Ni (dNi), and Zn (dZn) are classified as nutrient-type dissolved trace metals (dTMs) with vertical profiles similar to nutrients (phosphate (P), nitrate+nitrite (TN) or silicic acid (Si)) (Moore et al., 2013; Morel and Price, 2003). The close relationships between dTMs and nutrients are assumed to demonstrate the essential roles of these TMs in phytoplankton processes. For instance, Zn is a co-factor in a series of proteins, e.g., carbonic anhydrase and alkaline phosphatase (Morel et al., 1994; Tortell et al., 2000), and Zn availability can determine the access of phytoplankton to the dissolved organic phosphorus pool (Mahaffey et al., 2014). Nickel is primarily associated with urease and superoxide dismutase has a Ni-containing form (Dupont et al., 2010). Copper is used in photosynthetic and respiratory electron transport chains (La Fontaine et al., 2002; Twining and Baines, 2013). At

* Corresponding author.
E-mail address: eachterberg@geomar.de (E.P. Achterberg).

https://doi.org/10.1016/j.gca.2024.01.001
Received 13 June 2023; Accepted 2 January 2024
Available online 8 January 2024

excess concentrations, Cu can be toxic to phytoplankton (Lopez et al., 2019; Sunda, 1975). Cadmium can substitute for Zn in carbonic anhydrase in diatoms (Lane et al., 2005; Lane and Morel, 2000), or possibly, Cd is mistakenly assimilated into cells with other divalent metals (Horner et al., 2013). In addition to dissolved phases, a large fraction of TM inventory is hosted in particulate phases (particulate TM (pTM)), which can be assimilated by phytoplankton when the metals are sufficiently labile (Chen et al., 2022; Twining et al., 2015). Therefore, the supply of TMs in both dissolved and particulate forms to the euphotic zone may determine the structure and functioning of marine ecosystems (Lohan and Tagliabue, 2018; Morel and Price, 2003; Twining and Baines, 2013).

Nutrients and nutrient-type dTMs in the ocean typically show surface depletion due to phytoplankton uptake, and gradually increasing concentrations with depth due to remineralization of sinking organic particles (Lohan and Tagliabue, 2018). The similarities in nutrient and dTM profiles are manifested by linear dTM-nutrient relationships, with examples of strong dCd-P, dZn-Si, dCu-Si, and dNi-P correlations in oceanic waters (Bruland et al., 1978; Jacquot and Moffett, 2015; Lohan and Tagliabue, 2018; Middag et al., 2020). Specifically, the linear dCd-P relationship is ascribed to the uptake of Cd and P by phytoplankton and subsequent remineralization of phytoplankton debris following cell death with a release of Cd and P (Twining and Baines, 2013). Pronounced changes in slopes (kinks) of the dCd-P relationship are observed in the global oceans and have been attributed to a deeper regeneration of Cd relative to P (Boyle, 1988; Roshan and DeVries, 2021), enhanced Cd uptake relative to P by phytoplankton under Fe limitation (Cullen, 2006; Sunda and Huntsman, 2000), or mixing of water masses with contrasting Cd:P ratios (Middag et al., 2018; Xie et al., 2015). Nickel in the ocean is characterized by residual dNi concentrations of ~ 1.7 nM in surface waters (John et al., 2022). The variable dNi-nutrient relationships in the ocean are attributed to cellular variations in Ni:P ratios between phytoplankton species ((Twining and Baines, 2013), higher Ni requirements for diatoms and cyanobacteria (Archer et al., 2020), and/or water mass mixing (Chen et al., 2023; Middag et al., 2020). Profiles of dZn and Si showed strong resemblance, especially in deep waters (Cloete et al., 2019; Middag et al., 2019; Wyatt et al., 2014). Strong basin-scale correlations between dCu and Si were observed in the North Atlantic across the GEOTRACES GA03 transect (Jacquot and Moffett, 2015; Roshan and Wu, 2015a) and the Southern Ocean (Cloete et al., 2019). In addition to similarities in source strengths (e.g. fluvial, atmospheric, and benthic inputs), the resemblance between dCu, dZn and Si has been attributed to an enhanced uptake of Cu, Zn, and Si by diatoms and subsequent remineralization of sinking diatom cells (Cloete et al., 2019; Vance et al., 2017). There are still uncertainties regarding the processes that set the stoichiometric relationships between nutrient-type dTMs and nutrients in intermediate and deep waters, whilst this knowledge is essential for projecting the supply of nutrients and micronutrients to the euphotic zone, and hence primary productivity in a future ocean.

High latitude oceans are key regions for global thermohaline circulation. Elemental stoichiometries in Antarctic water masses are set in the Southern Ocean (Middag et al., 2020, 2018; Vance et al., 2017) due to a combined influence of high diatom productivity and subsequent remineralization and dynamic physical circulation. Nutrients and nutrient type dTMs with fixed ratios are exported from the Southern Ocean into low latitude nutrient-depleted waters and subsequently affect primary productivity (Middag et al., 2020; Sarmiento et al., 2004). Here, we present the first comprehensive investigation of the spatial distributions of nutrient-type TMs (Cd, Cu, Ni, and Zn) in both dissolved and particulate phases along a 40°S section in the South Atlantic Ocean. The study region is situated between the subtropical and sub-Antarctic front, and is characterized by elevated chlorophyll concentrations. Therefore, this region is an important transition zone between the nutrient-rich but Fe-depleted Southern Ocean, and nitrate and Fe depleted South Atlantic Subtropical Gyre (SASTG). As a part of the International GEOTRACES program (cruises GA10), we assess the sources of TMs and their relationships with nutrients. With the help of water mass analysis, we investigate the importance of water mass mixing on the distributions of nutrient-type dTMs along the 40°S section in the South Atlantic Ocean. A high sampling resolution of TMs and ancillary parameters allows us to explore in detail the mechanisms that control the stoichiometric relationships between nutrient-type dTMs and nutrients.

2. Materials and methods

2.1. Sampling and analyses

The study region is located along latitude 40°S in the South Atlantic Ocean, which is the transition zone between the SASTG and Southern Ocean (Fig. 1). Seawater samples were collected during two UK GEOTRACES GA10 cruises (D357 from October 18th to November 22nd, 2010 on board the *RRS Discovery*; JC068 from December 24th, 2011 to January 27th, 2012 on board the *RRS James Cook*). Full details of seawater sampling, nutrient analyses, and physical parameters (e.g., salinity, potential temperature [Θ], and dissolved oxygen [O_2]) can be found in the cruise reports (available as part of GEOTRACES Intermediate Data Product Group (IDP), 2021). In short, TM samples were collected using a titanium CTD rosette frame with 24 × 10 L trace metal clean Teflon-coated OTE (Ocean Test Equipment) Niskin bottles, following GEOTRACES sample handling protocols (Cutter et al., 2017). After recovery, the OTE bottles were processed in a class 100 clean laboratory, samples for dTMs were filtered through 0.2 μm polyethersulfone membrane filter capsules (AcroPak Supor, Pall). All samples were acidified to pH 1.7 by addition of 12 M hydrochloric acid (UpA, Romil). Particulate samples were collected from the OTE bottles onto acid cleaned 25 mm 0.45 μm Supor polyethersulfone membrane filters (Pall) and stored frozen (−20 °C) until shore-based analyses.

Upon return to the laboratory, dTM samples were 10-fold preconcentrated using an automated SeaFAST system (SC-4 DX SeaFAST pico; ESI) with online pH buffering and seawater sample matrix removal. Preconcentrated samples were then analyzed by high-resolution inductively coupled plasma-mass spectrometry (HR-ICP-MS; Thermo Fisher Element XR) using methods exactly as per Rapp et al. (2017). The accuracy and precision of the dTM measurements were evaluated by GEOTRACES reference materials with the results showing good agreement (Table 1). The labile particulate fraction was determined using the methods described in Berger et al. (2008). Determination of the total particulate fraction was carried out using a sequential acid digestion modified from Ohnemus et al. (2014) and described in detail in Milne et al. (2017). Both fractions were analyzed using ICP-MS (Thermo-Fisher X-Series 2) equipped with a collision cell utilizing 7 % H_2 in helium. Measured concentrations were blank corrected based on concentrations obtained from replicate analyses of acid washed blank filters (Table S1). Certified reference materials were used to assess digestion efficiency, with measured particulate data in good agreement with certified values (Table 2).

Samples for nutrients (P, TN, and Si) were collected alongside TMs, and were analyzed using an autoanalyzer (Bran & Luebbe AA III) (Woodward and Rees, 2001), with procedures as per GO-SHIP protocols (Becker et al., 2020). Salinity, temperature, depth, and O_2 depth profiles were measured using a Seabird 911+ CTD system on the rosette frame, including a SBE 43 O_2 sensor. The salinity (conductivity) sensor was calibrated by on-board analysis of discretely collected samples using an Autosal 8400B salinometer, and for the O_2 sensor calibration we used a photometric automated Winkler titration system.

2.2. Water mass analysis

Five water masses were identified in the study region, namely South Atlantic Central Water (SACW), Antarctic Intermediate Water (AAIW), Upper Circumpolar Deep Water (UCDW), North Atlantic Deep Water (NADW), and Antarctic Bottom Water (AABW) (Liu and Tanhua, 2021;

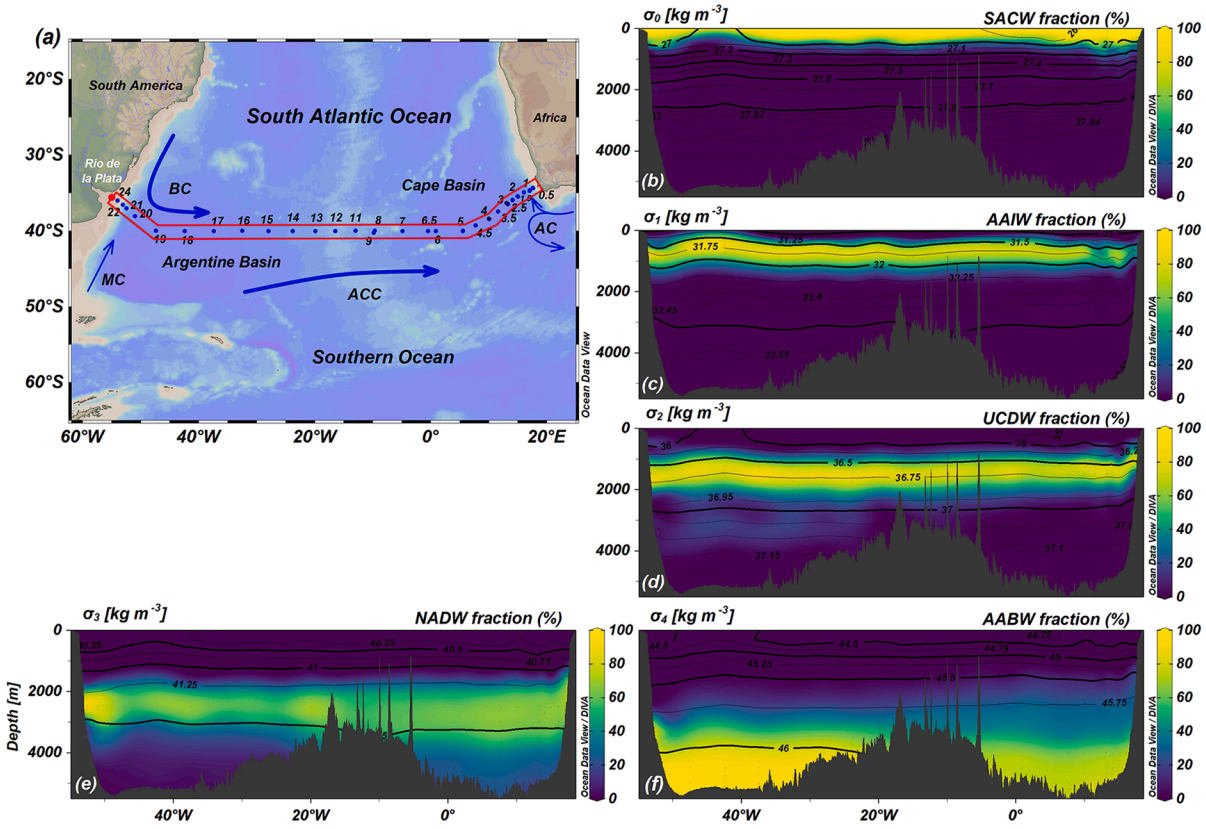

Fig. 1. (a) GA10 transect in the South Atlantic Ocean. Transect extends from the African coast to South American coast and crossed the Cape Basin and Argentine Basin. Major surface currents in this region include warm Agulhas current (AC) and Brazil Current (BC), cold Malvinas Current (MC) and Antarctic Circumpolar Current (ACC). Stations # 0.5–6 were sampled for nutrients and trace metals during the GEOTRACES D357 cruise, while stations # 7–24 and stations # 1–5 were investigated (or re-visited) during the JC068 cruise. (b–f) Estimated percentage contributions of South Atlantic Central Water (SACW), Antarctic Intermediate Water (AAIW), Upper Circumpolar Deep Water (UCDW), North Atlantic Deep Water (NADW), and Antarctic Bottom Water (AABW) along the transect. Note that surface waters with depths < 200 m and Θ > 10 °C were excluded from the water mass analysis.

Table 1
GEOTRACES reference material results for dissolved Cd, Ni, Cu, and Zn. Uncertainties are ± 1 SD.

	Cd (pmol kg^{-1})	Ni (nmol kg^{-1})	Cu (pmol kg^{-1})	Zn (nmol kg^{-1})
SAFe D1 measured	967 ± 49, n = 5	8.59 ± 0.62, n = 6	2.02 ± 0.07, n = 6	6.90 ± 0.56, n = 6
SAFe D1 consensus	991 ± 31	8.58 ± 0.26	2.27 ± 0.11	7.40 ± 0.35
SAFe D2 measured	949 ± 66, n = 20	8.60 ± 0.36, n = 19	2.15 ± 0.16, n = 22	7.27 ± 0.22, n = 7
SAFe D2 consensus	986 ± 23	8.63 ± 0.25	2.28 ± 0.15	7.43 ± 0.25
SAFe S measured		2.56 ± 0.55, n = 25	0.55 ± 0.06, n = 30	0.064 ± 0.021, n = 6
SAFe S consensus		2.28 ± 0.09	0.52 ± 0.05	0.069 ± 0.010
GEOTRACES S measured		2.54 ± 0.30, n = 6	0.86 ± 0.05, n = 7	
GEOTRACES S consensus		2.08 ± 0.06	0.84 ± 0.06	
GEOTRACES D measured	263 ± 4, n = 3	4.16 ± 0.12, n = 3	1.65 ± 0.06, n = 3	1.71 ± 0.10, n = 2
GEOTRACES D consensus	271 ± 6	4.00 ± 0.10	1.62 ± 0.07	1.71 ± 0.12

Stramma and England, 1999; Wyatt et al., 2014). Percentage contributions of water masses along the GA10 transect were quantified using optimum multiparameter (OMP) analysis (Karstensen and Tomczak, 1998; Tomczak and Large, 1989). Depths < 200 m and Θ > 10 °C were excluded from the OMP analysis to avoid the influence of surface biological processes on nutrient concentrations. Endmember Θ, salinity, and nutrient values of each water mass were pre-determined by property-property plots that corresponded to the water mass characteristics (Fig. S1). The defined endmember values of water masses in this study (Table 3) correspond to reported ranges for the South Atlantic Ocean (Larqué et al., 1997; Middag et al., 2018; Schlosser et al., 2019). Since water masses evolve during their lateral transport, water mass characteristics reflect their local properties rather than those from their physical formation regions. Note that water types that contribute to certain water masses, for example Labrador Sea Water and Denmark Strait Overflow Water for NADW, are not identified in this study. Therefore, the endmember characteristics here refer to the specific properties of water masses that can be distinguished in our study region.

Endmember dTM levels of water masses (Table 3) were predicted using a fit linear regression model in the program *R* (version 4.2.0) (standard errors reported). All predictions were accompanied by correlation coefficients > 0.98 (for dCd, dCu, and dNi = 0.992), demonstrating the reliability of the endmember calculations. Spatial distributions of dTMs and nutrients along the GA10 transect were reconstructed by direct multiplication of water mass fractions with their endmember compositions. The differences between measured and reconstructed values are defined as residuals. The uncertainties of water mass contributions of the OMP analysis were estimated by summing the residuals of temperature, salinity, O_2, and nutrients scaled by their weights, as per Evans et al. (2020). The results indicated that water mass contributions in most samples were calculated with uncertainties of < ± 0.1 (Fig. S2). In addition, critical points about the emergence and maximum occurrence of water masses (e.g., maximum occurrences of AAIW, UCDW, and NADW at $\sigma_0 \sim 27.1$ kg m^{-3}, $\sigma_0 \sim 27.58$ kg m^{-3}, and $\sigma_4 \sim 45.8$ kg m^{-3}, respectively; disappearances of SACW and UCDW at

Table 2
Results from the digestion and analysis of certified reference materials for particulate trace metals. The measured values are the mean of 3 replicate analyses with uncertainties of ± 1 SD. All values are in mg kg^{-1}.

Reference material		BCR-414	SO-2	LKSD-4	IAEA-433
Al	Certified	n/a	80700 ± 1800	n/a	78200 ± 4200
	Measured		87000 ± 840		94900 ± 695
	% Recovery		108		121
Cd	Certified	0.383 ± 0.014	n/a	1.9	n/a
	Measured	0.438 ± 0.100		2.3 ± 0.6	
	% Recovery	114		120	
Cu	Certified	29.5 ± 1.3	n/a	31	30.8 ± 2.6
	Measured	30.0 ± 2.3		30 ± 1	34.0 ± 2.0
	% Recovery	102		96	111
P	Certified	n/a	3000 ± 200	n/a	n/a
	Measured		3800 ± 240		
	% Recovery		128		
Ni	Certified	18.8 ± 0.8	8 ± 2	31	39.4 ± 3.1
	Measured	24.1 ± 3.4	6 ± 1	36 ± 1	47.0 ± 2.0
	% Recovery	128	74	116	120
Zn	Certified	111.6 ± 2.5	124 ± 5	194	101 ± 8
	Measured	113.0 ± 1.1	131 ± 6	178 ± 10	111 ± 3
	% Recovery	101	106	92	109

n/a = either no certified value or the element was not determined during analysis.

$\sigma_0 \sim 27.25$ kg m^{-3} and $\sigma_2 \sim 36.9$ kg m^{-3}, respectively; Fig. 1) are almost identical when weights and stoichiometries of pre-defined nutrient endmember values are varied by 5 %. These critical points, rather than the absolute fractions of water masses, are essential for our discussion on the relationships between nutrients and dTMs. Furthermore, previous work has demonstrated that OMP could be a robust method to assess the importance of water mass mixing and local remineralization on the distributions of dCd, dNi, and dZn in the ocean (Middag et al., 2020, 2019, 2018; Quay and Wu, 2015; Roshan and Wu, 2015b).

2.3. Figures and statistical analysis

Figs. 1, 2, 3, 4, and 8, and Fig. S9 and S10 were created with Ocean Data View (ODV; version 5.6.2) software (Schlitzer, 2021) using DIVA gridding. Fig. 5 was created with ODV using quick gridding. Fig. 10 was created based on a map obtained from ODV. All other plots and associated statistical analyses were performed by *R* (version 4.2.0) with packages *tidyverse* (Wickham et al., 2019) and *ggpmisc* (Aphalo, 2022).

3. Results

3.1. Hydrography

Surface waters along the GA10 transect mainly consisted of cold and fresh Sub-Antarctic Surface Water (SASW) at longitudes between 10°W–5°E and 42–47°W, and warm and salty Sub-Tropical Surface Water (STSW) at longitudes between 10 and 42°W, west of 47°W, and east of 5°E. The SASW was characterized by $\Theta < 12.5$ °C, and STSW by $\Theta > 12.5$ °C (Fig. 2). The STSW west of 50°W was influenced by the Brazil Current (BC) at depths down to ~ 300 m. These surface waters were defined as S-BC ("S" stands for "surface"). The STSW east of 10°E was affected by the Agulhas Current (AC) at depths down to ~ 400 m; surface water in region was assigned as S-AC. Both BC and AC and their surface waters were characterized by elevated salinities (>35) and Θ (>15 °C) (Fig. 2).

The predicted fractions of water masses (Fig. 1) at depths > 500 m are consistent with reported indications for the SASTG (Arhan et al., 2003; Liu and Tanhua, 2021; Schlosser et al., 2019). From below the surface currents to depths of ~ 1000 m (potential density σ_0 of ~ <27.25 kg m^{-3}), the water column was characterized by gradually decreasing SACW and increasing AAIW fractions. The maximum contribution of AAIW occurred at σ_0 of ~ 27.1 kg m^{-3} (depth of ~ 800 m). Below AAIW, deep waters consisted of cold, nutrient-rich, oxygen-depleted UCDW. The maximum UCDW fraction was identified at σ_0 ~ 27.58 kg m^{-3} (depth ~ 1500 m). The influence of UCDW diminished at σ_2 of ~ 36.9 kg m^{-3}, consistent with Stramma and Peterson (1990). Deep waters at depths > 2000 m mainly consisted of NADW and AABW. The NADW was transported with the Deep Western Boundary Current (DWBC) from the Northern Hemisphere to the South Atlantic Ocean. The core of the southbound NADW was identified at a depth of ~ 2500 m (σ_4 of ~ 45.8 kg m^{-3}). Below NADW, bottom waters consisted of cold and nutrient-rich AABW.

3.2. Distributions of TMs and nutrients

Vertical distributions of nutrients and dTMs along the transect are in excellent agreement with reported observations at crossover stations from other GEOTRACES cruises (GEOTRACES Intermediate Data Product Group, 2021; Middag et al., 2019; Wyatt et al., 2021, 2014) and our data have met the GEOTRACES intercalibration procedures and are available in the GEOTRACES IDP2021. Specifically, our dCu data are consistent with those reported by (Little et al., 2018) for samples collected from the same cruises. Our dNi and dZn data are in agreement with data from (Archer et al., 2020) and (Wyatt et al., 2014), who determined dNi and dZn using isotope dilution with ICP-MS detection and flow injection with fluorometric detection, respectively (Fig. S3). All nutrients and dTMs showed increasing concentrations with depth (Fig. 2). For instance, dCd and dCu concentrations increased from 14.8 ± 6.6 pmol kg^{-1} (n = 14) and 0.817 ± 0.605 nmol kg^{-1} (n = 15) at depths < 20 m to 415 ± 126 pmol kg^{-1} (n = 21) and 0.934 ± 0.171 nmol kg^{-1} (n = 21) at a depth of ~ 500 m, respectively. The SASW generally demonstrated higher nutrient and dTM concentrations (P > 0.5 μmol kg^{-1}, dCu > 0.5 μmol kg^{-1}, dNi > 3.0 μmol kg^{-1}) than STSW (e.g., P < 0.5 μmol kg^{-1}, dZn < 0.1 μmol kg^{-1}) at similar depth ranges. Both S-BC and S-AC showed lower nutrient concentrations (e.g., P < 0.2 μmol kg^{-1}) than other surface waters (depths < 200 m). In contrast, dCu (>0.7 nmol kg^{-1}) and dZn levels (up to 2.1 nmol kg^{-1}) were dramatically elevated in both near shore regions. In addition, surface waters associated with lower salinities near the Rio de la Plata on the western side of the transect showed elevated nutrient and dTM levels (e.g., dCu > 0.6 nmol kg^{-1}, dNi > 4 nmol kg^{-1}, and P > 1 μmol kg^{-1}).

Trends in nutrient and dTM concentrations at depth were related to changes in water mass fractions (Fig. 3). Nutrient and dTM concentrations increased with depth through the SACW and AAIW layers and reached intermediate maxima in the core of UCDW (~depth 1500 m) (Table 4). Below the UCDW, nutrient and dTM concentrations decreased with increasing NADW contributions from 1500 m to ~ 2500 m. The core of the NADW (σ_4 ~ 45.8 kg m^{-3}) exhibited relatively depleted nutrient and dTM concentrations with respect to UCDW. At depths > 2500 m, all nutrients and dTMs showed increasing concentrations with depth and AABW fractions. When compared with UCDW, AABW showed much higher concentrations of Si, dCu, and dZn, and similar levels of P,

Table 3
Pre-defined temperature (Θ), salinity, oxygen, phosphate (P), nitrate+nitrite (TN), and silicic acid (Si) concentrations, and calculated dissolved trace metal (dCd, dCu, dNi, dZn) concentrations (with 95 % confidence levels) of water masses in the South Atlantic Ocean. SACW: South Atlantic Central Water, AAIW: Antarctic Intermediate Water, UCDW: Upper Circumpolar Deep Water, NADW: North Atlantic Deep Water, and AABW: Antarctic Bottom Water. Endmember concentrations predicted by previous work (with similar Θ-S ranges to this study) are shown for comparison.

Water mass	Location*	Θ (°C)	Salinity	Oxygen (μmol kg^{-1})	P (μmol kg^{-1})	TN (μmol kg^{-1})	Si (μmol kg^{-1})	dCd (nmol kg^{-1})	dNi (nmol kg^{-1})	dCu (nmol kg^{-1})	dZn (nmol kg^{-1})
SACW[1]	GA10	10	34.87	240	1.16 ± 0.03	15.6 ± 0.4	2.59 ± 0.68	0.134 ± 0.018	4.12 ± 0.14	0.687 ± 0.056	0.060 ± 0.210
	GA02[2]	10	34.80	285 ± 10	0.73 ± 0.01	12.0 ± 2.0	4.0 ± 3.0	0.070 ± 0.004	3.74 ± 0.03		0.01–0.29
AAIW	GA10	3.68	34.10	260	2.02 ± 0.04	29.6 ± 0.5	14.5 ± 0.6	0.572 ± 0.012	5.76 ± 0.09	1.01 ± 0.04	1.44 ± 0.13
	GA02	3.80	34.05	270 ± 7	1.78 ± 0.01	25.0 ± 1.0	13.0 ± 2.0	0.527 ± 0.004	5.59 ± 0.02		1.16–1.29
	GA02-N[3]							0.535	5.25		1.35
UCDW	GA10	2.80	34.60	170	2.35 ± 0.03	35.0 ± 0.5	66.4 ± 0.7	0.796 ± 0.010	6.97 ± 0.08	1.72 ± 0.03	4.73 ± 0.12
	GA02	2.6	34.75	170 ± 5	2.35 ± 0.01	35.0 ± 0.2	65.0 ± 5.0	0.823 ± 0.007	7.29 ± 0.05		5.01–5.16
NADW	GA10	3.60	34.94	230	1.42 ± 0.02	21.6 ± 0.4	26.9 ± 2.4	0.333 ± 0.011	5.43 ± 0.09	1.50 ± 0.03	2.04 ± 0.13
	GA02-N [4]							0.342	4.79		2.43
	GA03[5]								4.65 ± 1.69	1.74	2.00
AABW	GA10	0.24	34.66	220	2.36 ± 0.01	33.2 ± 0.2	128 ± 1	0.797 ± 0.009	7.71 ± 0.07	3.36 ± 0.03	7.68 ± 0.10
	GA02	−0.1	34.66	210 ± 4	2.30 ± 0.01	33.0 ± 0.8	125.0 ± 4.0	0.783 ± 0.002	7.72 ± 0.02		7.67–7.69
	GA02-N [6]							0.834	7.24		7.03
	GA03[5]	0.18	34.702		2.16	30.68	116.5	0.763	7.66 ± 3.91	4.91	7.17
	GA08[7]	0.24	34.62		2.58 ± 0.22	36.4 ± 5.3	120 ± 10	1.02 ± 0.15	7.67 ± 0.94	3.57 ± 0.63	
Weight		24	24	2	8	8	8				

* Locations: GA10: this study, mainly along the 40 °S; GA02: along the west Atlantic Ocean; GA02-N: latitude > 0 °N along the GA02 transect; GA03: North Atlantic with latitudes of 15–40 °N; GA08: Southwest Atlantic with latitudes of 28.8–3 °S.

[1] The temperature of SACW was set as 10 °C to exclude the influence of surface currents and surface biological processes. Predefined endmember concentrations were estimated from property-property (e.g., Θ–S) plots.

[2] Predicted by Middag et al., (2018, 2019, 2020) using eOMP analyses.

[3] GA02-N: Endmember values estimated for GA02 samples in the North Atlantic Ocean. dCd: Middag et al. (2018), using equation 5 (dCd = 0.354*P–180) in their Fig. 3b and endmember P of 2.02 μM. dNi: Middag et al. (2020), using the NADW/NACW – AAIW mixing equation (dNi = 2.3*P + 0.6) and endmember P of 2.02 μM. dZn: Middag et al. (2019), using the Zn-Si relationship for SACW-AAIW mixing (dZn = 0.09*Si + 0.04). Endmember P and Si of AAIW during these calculations were 2.02 and 14.5 μM, respectively, in accordance with this study.

[4] dCd: Middag et al. (2018), using equation 3 (dCd = 0.287*P – 66) in their Fig. 3b. dNi: Middag et al. (2020) using the NADW – AABW mixing equation (dNi = 2.6*P + 1.1). dZn: Middag et al. (2019) using the Zn-Si correlation for NADW (dZn = 0.07*Si + 0.55). Endmember P and Si of NADW during these calculations were 1.42 and 26.9 μM, respectively, in accordance with this study.

[5] Θ, salinity, and nutrients: Jenkins et al. (2015) based on observations at WOCE A07 station 76. dCd: Roshan and Wu (2015a), endmember dCd from conservative mixing (their Table 1). dCu: Roshan and Wu (2015b), dCu = 0.0353*Si + 0.7991, R^2 = 0.78. dNi: IDP2021, deep water dNi-Si relationship, R^2 = 0.233, n = 34, predicted in 95 % confidence levels. dZn: Roshan and Wu (2015c), dZn = 0.0577*Si + 0.4484, R^2 = 0.756, n = 497. Endmember Si of NADW and AABW were set as 26.9 and 116.5 μM, respectively, in accordance with that defined by Jenkins et al. (2015).

[6] dCd: Middag et al. (2018) using equation 4 (dCd = 0.491*P – 325) in their Fig. 3b. dNi: Middag et al. (2020) using the NADW – AABW mixing equation (dNi = 2.6*P + 1.1). dZn: Middag et al. (2019) using the Zn-Si correlation for AABW NH (dZn = 0.05*Si + 0.63). Endmember P and Si of AABW during these calculations were 2.36 and 128 μM, respectively, in accordance with this study.

[7] raw data from (Liu et al., 2022a, 2022b). Endmember salinity and nutrient values were estimated from their correlations with Θ. Endmember dTM concentrations were predicted from their linear equations with Si. All values were calculated with 95% confidence levels.

TN, dCd, and dNi (Table 4). At depths between ~ 2000–3200 m, lower nutrient and dTM concentrations were observed at stations #20 and #21 (indicated on Fig. 3) compared to other stations. In addition, stations (#2, #5, and #6) on the eastern side of the transect (longitude 5°W–20°E) showed elevated dZn (>6 nmol kg^{-1}), dNi (>7 nmol kg^{-1}), and dCu (>2 nmol kg^{-1}) concentrations at depths between 1500 and 2000 m.

Prominent enrichments of pP (e.g., total pP 50–200 nmol kg^{-1}), pCd (total pCd > 10 pmol kg^{-1}), and pNi (total pNi > 50 pmol kg^{-1}) were observed in surface waters with depths < 100 m, in both labile and total particulate forms (Fig. 4). In contrast, elevated pCu and pZn levels were only associated with S-AC and S-BC. The S-BC near the Rio de la Plata also showed greatly increased concentrations of pAl (e.g., total pAl up to 1000 nmol kg^{-1}) and pNi (total pNi up to 250 pmol kg^{-1}). All the intermediate and deep waters with depths 200–4000 m were characterized by strongly depleted pTM concentrations (Fig. 5). Between 52 and 32°W in the Argentine Basin, strongly increased total pAl (57.8–584 nmol kg^{-1}), total pNi (20.5–156 pmol kg^{-1}), total pCu (80.0–485 pmol kg^{-1}), and total pZn concentrations (44.9–415 pmol kg^{-1}) were observed at depths > 4500 m. Labile particulate TMs also illustrated elevated concentrations in bottom waters in the Argentine Basin (Fig. 5).

3.3. Relationships between dTMs and nutrients

Nutrients and dTMs which show significant correlations with P are classified as a P group (dCd, dNi, and TN), and those with linear correlations with Si as a Si group (dCu and dZn) (Fig. 6). In this study, we use "-" to indicate the relationships between dTMs and nutrients, "/"to indicate the spot ratios (e.g., dCd/P), and ":" to demonstrate ratios associated with slopes (e.g., dCd:P), e.g., uptake and remineralization ratios, and ratios in dTM and nutrient changes due to water mass mixing. Both dCd – P and dNi – P relationships illustrated changes in slopes

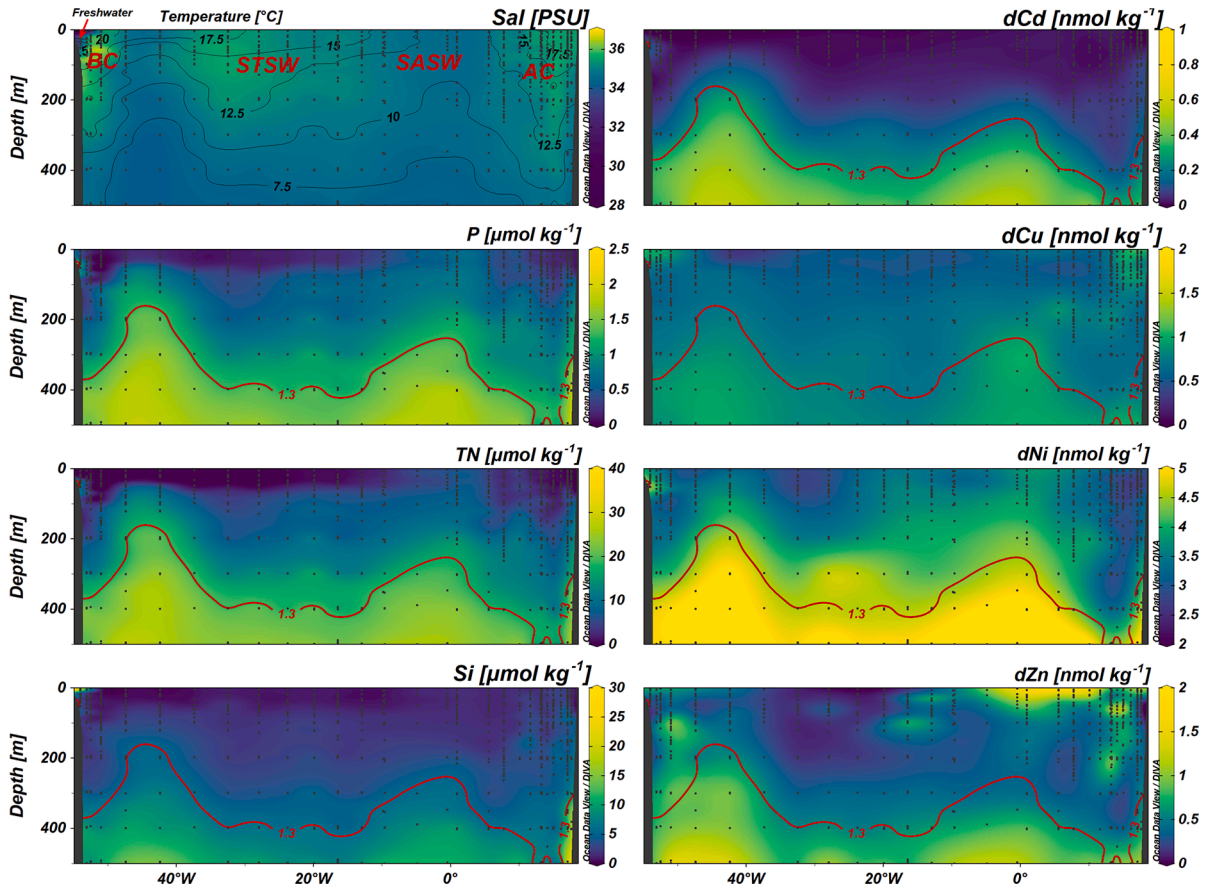

Fig. 2. Distributions of salinity, nutrients (phosphate (P), nitrate+nitrite (TN), and silicic acid (Si)), and nutrient-like dissolved trace metals (dCd, dCu, dNi, and dZn) at depths < 500 m along the GA10 transect. BC: Brazil Current; AC: Agulhas Current; SASW: Sub-Antarctic Surface Water; STSW: Sub-Tropical Surface Water. Contours of P at 1.3 µmol kg-1 are shown as red lines.

(kinks) at P concentrations of ~ 1.0–1.3 µmol kg^{-1}. The dNi – P kink is less prominent than the dCd – P kink. The overall dNi – P correlation was characterized by a slope of ~ 2.05 nmol/µmol (i.e., dNi:P = 2.05 × 10^{-3}). This ratio is similar to dNi:P values of deep waters in the Atlantic Ocean (e.g., AABW, UCDW, and NADW) (Middag et al., 2020; Schlitzer et al., 2018). The dCd:P ratios calculated from the linear dCd-P correlation at P < 1 µmol kg^{-1} and P > 1 µmol kg^{-1} were 0.092 × 10^{-3} and 0.506 × 10^{-3}, respectively. The latter ratio is consistent with elevated dCd:P ratios in the South Atlantic Ocean (Middag et al., 2018; Xie et al., 2015).

The vertical distributions of dCu and dZn strongly resembled those of Si in the South Atlantic, in agreement with other studies (Lohan and Tagliabue, 2018; Roshan and Wu, 2015a; Vance et al., 2017; Wyatt et al., 2014). By excluding large variations in surface waters, the overall dZn-Si relationship was characterized by a slope of ~ 0.06 × 10^{-3} without appearances of kinks. The overall dCu-Si correlation had a slope of ~ 0.02 × 10^{-3} and showed a slight zigzag-shaped change at Si of ~ 60 µmol kg^{-1}. The inferred dZn:Si and dCu:Si ratios along the transect are close to reported values for the Atlantic Ocean (Zn:Si = 0.05–0.08 × 10^{-3}; Cu:Si = 0.03–0.05 × 10^{-3}) (Boye et al., 2012; Wyatt et al., 2014; Roshan and Wu, 2015b, c; Middag et al., 2019).

4. Discussion

4.1. Nutrients and TMs in surface waters along transect GA10

Stations along transect GA10 showed increasing nutrient and dTM concentrations with depth down to 500 m (Fig. 2). The negative intercept (-2.62 µmol kg^{-1}) of the TN-P relationship (Fig. S4) in these waters is typical for the South Atlantic Ocean and consistent with TN being the primary limiting nutrient for primary productivity in the region (Browning et al., 2014b; Moore et al., 2013). The relationships for dCd-P, dNi-P, and Si-P were significant in the upper 500 m (Fig. S4). A majority of samples showed a significant relationship between dCu and P. The dNi-P relationship showed a consistent slope in the upper waters over the full P concentration range. In contrast, kinks at P of ~ 1.3 µmol kg^{-1} were observed for the dCd-P, dZn-P, and Si-P relationships. At P > 1.3 µmol kg^{-1}, similar patterns of dTM-nutrient relationships were observed at depths < 500 m and between 500 and 1000 m (Fig. 6). Therefore, the nutrient and dTM stoichiometry in the upper 500 m with P > 1.3 µmol kg^{-1} was largely determined by similar processes as at greater depths. These processes, likely include water mass mixing rather than local biological processes (Middag et al., 2018).

Significant spatial variations in the distributions of dTMs and nutrients were observed in the upper 500 m with P < 1.3 µmol kg^{-1} (Fig. 2, Fig. 4). Total pTM concentrations in surface waters were significantly correlated with total pP, showing high correlation coefficients for total pCd, pNi, and pCu (Fig. 7). By excluding the samples with significant contribution of lithogenic particles (total pAl/pP > 0.5), the Cd:Ni:Cu:Zn:P stoichiometry in surface water particles was 0.143 ± 0.015: 1.97 ± 0.21: 0.513 ± 0.065: 2.00 ± 0.62: 1000. This stoichiometry is in agreement with the reported average elemental composition of marine phytoplankton (Cd:Ni:Cu:P = 0.21:1.4:0.38:1000) (Ho et al., 2003; Twining and Baines, 2013), and represents the uptake stoichiometry of local phytoplankton communities. All dTMs in surface waters showed decreasing concentrations with total pP (Fig. S5), demonstrating that surface dTMs were influenced by phytoplankton uptake and remineralization processes. Specifically, the linear relationships between dTMs (except dZn) and P had the steepest slopes in SASW (Fig. S6). The dCd:P

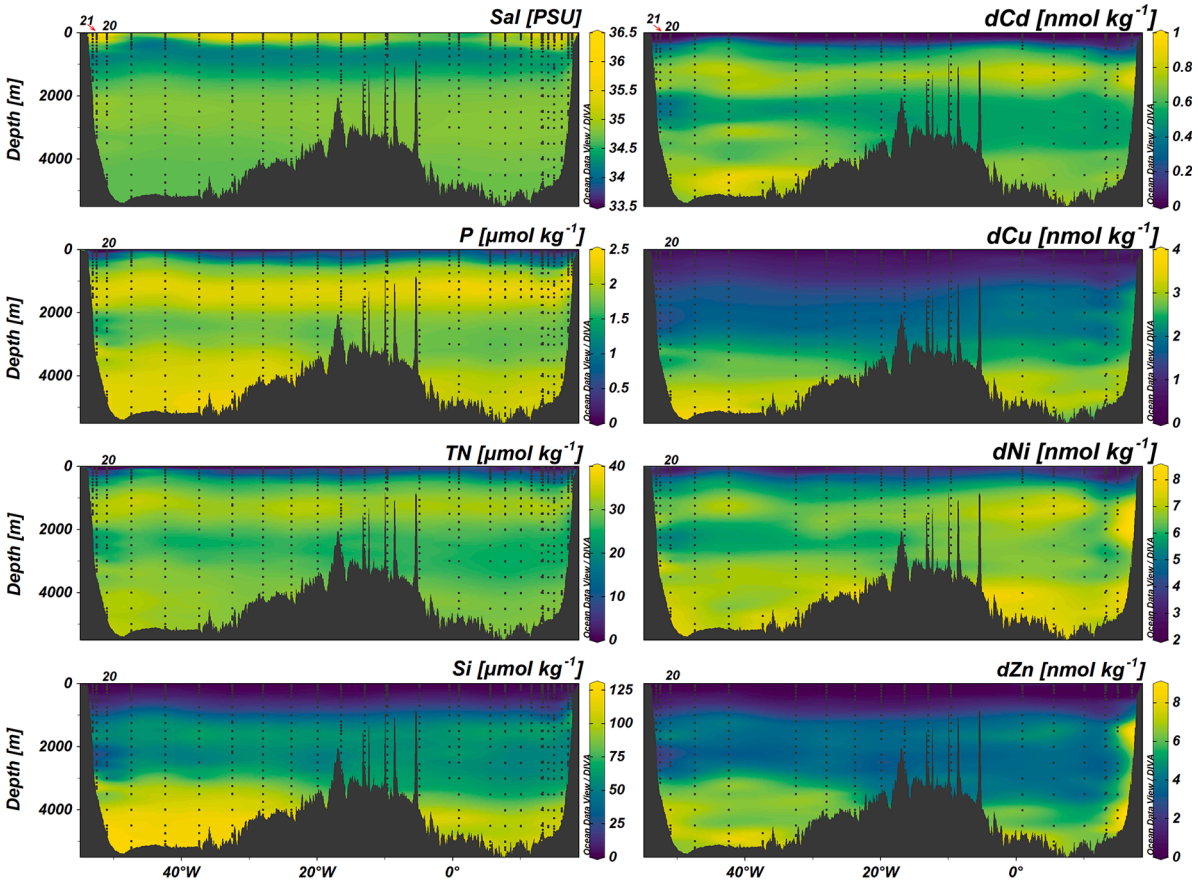

Fig. 3. Full-depth section profiles of nutrients (phosphate (P), nitrate + nitrite (TN), and silicic acid (Si)), and nutrient-type dissolved trace metals (dCd, dCu, dNi, and dZn) along the GA10 transect. Stations #21 and #22 with lower levels of nutrients and dTMs at 2000–3200 m are labeled.

(0.25×10^{-3}), dCu:P (0.33×10^{-3}), and dNi:P (1.50×10^{-3}) ratios were comparable to the uptake stoichiometry of marine phytoplankton, reflecting a control of these elements by phytoplankton in the SASW. The consistently lower y-intercepts in the SASW compared to other upper waters indicate that there was residual P (~0.5 µmol kg^{-1} from the dCd-P correlation) relative to dTMs, consistent with the elevated uptake stoichiometries of Si and dTMs relative to P by diatoms in the nutrient-rich Southern Ocean (Twining and Baines, 2013; Vance et al., 2017). The dTM-P relations showed the lowest slopes in STSW with relatively low correlation coefficients (Fig. S6), suggesting that distributions of dTMs and nutrients in STSW were additionally affected by processes other than phytoplankton activities, e.g. water mass mixing.

Surface waters in near-shore regions (S-AC and S-BC) showed strong dTM and pTM enrichments (Fig. 2, Fig. 4). The dTM concentrations generally increased with total pAl levels (Fig. S5), indicating that lithogenic particles are an additional source of dTMs. Specifically, pronounced enrichments of pCu, pNi, and pZn were observed in S-BC (Fig. 4), accompanied by dTM enrichments. Refractory pTM concentrations, calculated from total pTM – labile pTM, illustrated significant correlations with refractory pAl, especially for S-BC samples (Fig. S7). The estimated ratios of refractory pCu:pAl (~0.12×10^{-3}), pNi:pAl (~0.13×10^{-3}), and pZn:pAl (~0.36×10^{-3}) were similar to Upper Continental Crust (UCC) values (Cu:Ni:Zn:Al = 0.15:0.26:0.34:1000) (Rudnick and Gao, 2003), demonstrating that riverine materials from the Rio de la Plata provided additional pTMs to near-shore regions. Potentially through the dynamic exchange between dissolved and particulate phases (Chen et al., 2022; Homoky et al., 2012), surface dCu and dNi enrichment in S-BC relative to P was observed in waters with lower salinities (Fig. S5). The sporadically high dZn levels in S-BC were also potentially ascribed to the input of riverine materials, which yielded a dZn-P relationship with a poor correlation coefficient ($R^2 < 0.01$). In addition, dNi enrichment associated with waters with higher salinities were observed in the S-BC, suggesting that the excess dNi (possibly originally derived from freshwater discharge) was carried by the warm and salty BC flowing along South America.

Dissolved Cu and dZn in the S-AC exhibited increasing concentrations with decreasing P (Fig. S6), suggesting that AC is a source of surface dCu and dZn to our study region (Gosnell et al., 2012; Wyatt et al., 2014). This is probably caused by enhanced supply of Zn and Cu by atmospheric dry and wet deposition in the South Indian Ocean, and Southeast Atlantic (Chance et al., 2015). Atmospheric contributions of dCd and dNi were not identified in the S-AC, possibly due to the low Ni and Cd concentrations in aerosols (Chance et al., 2015). The pTM enrichments in the S-AC (Fig. 4) were not accompanied by elevated pAl concentrations, and most samples in the S-AC showed low RpTM levels (Fig. S7) and significant correlations between pTMs and pP (Fig. 7). Therefore, pTMs in the S-AC were mainly associated with biogenic rather than lithogenic particles. The pTM enrichments in the S-AC can also be supplied by lateral advection of metal-enriched waters from the AC and/or the South African continental shelf (Wyatt et al., 2021).

The distribution of dTMs was further studied in detail in surface water samples collected by the tow fish at water depths of 2–3 m (Fig. S8). Dissolved Cu (generally > 0.6 nmol kg^{-1}) was higher in the tow fish samples than in the upper waters sampled by the CTD, reflecting atmospheric input of dCu (Chance et al., 2015). As a result of phytoplankton uptake, dCd (14.7 ± 6.6 pmol kg^{-1}, n = 84) and dZn (0.154 ± 0.110 nmol kg^{-1}, n = 80) were present at very low levels in the tow fish samples, and lower than the dCd and dZn ranges in waters immediately below (depth 10–500 m). Atmospheric inputs for dZn were not obvious in tow fish samples, possibly due to the large variations in Zn

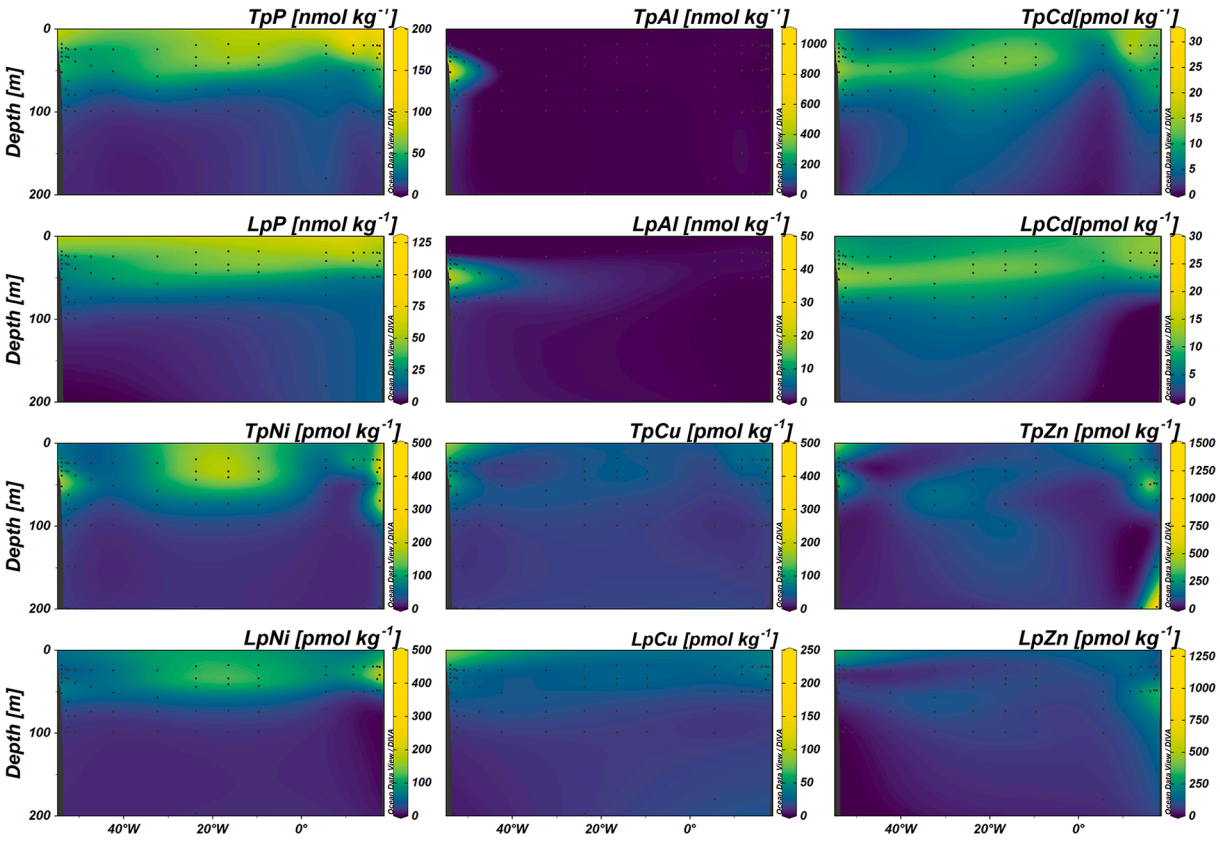

Fig. 4. Sections of labile and total particulate P, Al, Cd, Ni, Cu, and Zn at depths < 200 m along the GA10 transect.

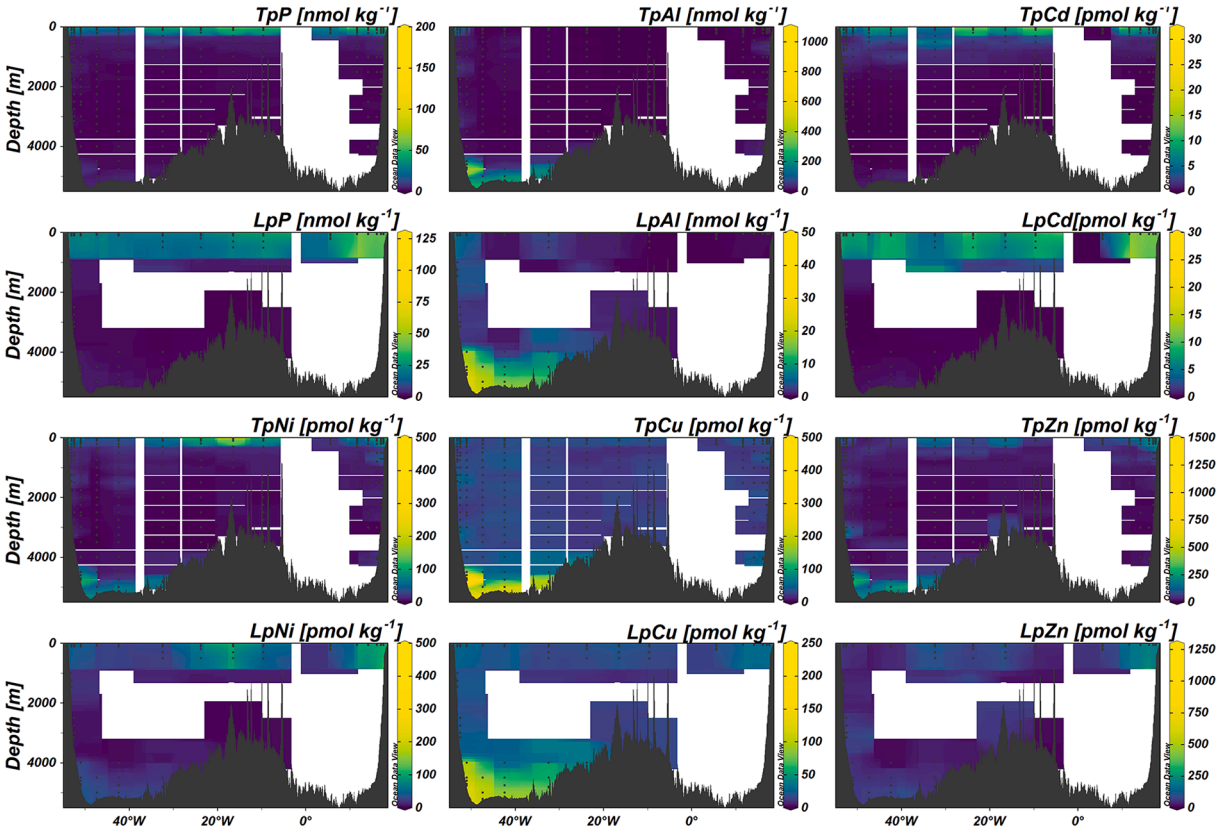

Fig. 5. Full-depth section profiles of total particulate (total p) and labile particulate (labile p) P, Al, Cd, Ni, Cu, and Zn along the GA10 transect.

Table 4
Concentrations of nutrients (phosphate (P), nitrate+nitrite (TN), and silicic acid (Si)) and nutrient-type dissolved trace metals (dCd, dCu, and dZn) in waters of the Weddell Gyre (WG, 56–62 °S), Antarctic Zone (AZ, 50–56 °S), Polar Front Zone (PFZ, latitude 45–50 °S), and sub-Antarctic Zone (SAZ, latitudes 41–45 °S). Data were calculated from the GIPY04 and GIPY05 transects along the zero meridian (Cloete et al., 2019; Croot et al., 2011; GEOTRACES IDP 2021). The observed concentrations of UCDW (Upper Circumpolar Deep Water) core, NADW (North Atlantic Deep Water) core, and bottom maximum of AABW (Antarctic Bottom Water) along the GA10 transect are shown for comparison.

Waters	P (μmol kg^{-1})	TN (μmol kg^{-1})	Si (μmol kg^{-1})	dCd (pmol kg^{-1})	dNi (nmol kg^{-1})	dCu (nmol kg^{-1})	dZn (nmol kg^{-1})
WG, depths < 100 m	1.84 ± 0.10, n = 22	26.7 ± 1.5, n = 22	65.6 ± 5.1, n = 22	667 ± 189, n = 2		1.48 ± 0.31, n = 2	2.70 ± 0.75, n = 2
WG, depths > 3000 m	2.26 ± 0.02, n = 424	32.6 ± 0.4, n = 402	122 ± 7, n = 424	782 ± 40, n = 20		2.87 ± 0.37, n = 10	5.85 ± 0.85, n = 12
AZ, depths < 100 m	1.65 ± 0.13, n = 113	25.2 ± 1.3, n = 37	29.4 ± 18.5, n = 121	519 ± 138, n = 12		1.11 ± 0.17, n = 4	2.24 ± 0.51, n = 6
AZ, O_2 < 180 μmol kg^{-1}, Θ 1.5–2.5 °C	2.33 ± 0.07, n = 110	33.7 ± 1.1, n = 90	80.3 ± 9.6, n = 113	798 ± 35, n = 5		1.90 ± 0.48, n = 4	4.30 ± 0.46, n = 4
PFZ, depths < 100 m	1.35 ± 0.11, n = 88	19.6 ± 1.7, n = 16	1.31 ± 1.51, n = 102	262 ± 102, n = 18		0.795 ± 0.151, n = 7	0.570 ± 0.150, n = 9
SAZ, depths < 100 m	0.867 ± 0.277, n = 93	12.4 ± 2.3, n = 25	1.00 ± 1.17, n = 102	30.8 ± 37.6, n = 11			
UCDW core	2.24 ± 0.07, n = 177	32.5 ± 1.1, n = 117	58.9 ± 4.9, n = 117	721 ± 61, n = 32	6.73 ± 0.43, n = 32	1.64 ± 0.15, n = 32	4.22 ± 0.74, n = 32
NADW core	1.72 ± 0.10, n = 64	25.4 ± 1.3, n = 64	53.5 ± 7.8, n = 64	489 ± 60, n = 18	5.95 ± 0.45, n = 18	1.87 ± 0.17, n = 18	3.63 ± 0.66, n = 18
AABW maximum	2.21 ± 0.09, n = 134	31.2 ± 1.3, n = 134	112 ± 10, n = 134	739 ± 76, n = 43	7.42 ± 0.36, n = 43	3.15 ± 0.22, n = 43	7.02 ± 0.85, n = 41

concentrations in aerosol and rainwaters (from below detection limits to 541 pmol m^{-3}) both spatially and temporally (Chance et al., 2015). Dissolved Ni in the tow fish samples varied between 2.5 and 4.5 nmol kg^{-1}, showing an average (3.31 ± 0.38 nmol kg^{-1}, n = 83) which was comparable to the dNi range in the upper waters sampled by CTD. Maxima in dCd, dNi, and dZn were observed in SASW, coinciding with relatively low primary productivity (as indicated by fluorescence measurements). In contrast, dTM maxima in the S-AC and S-BC (and SASW near S-BC) were accompanied by strongly elevated fluorescence signals, indicating that nutrients and dTMs delivered by fluvial and atmospheric inputs and/or offshore transport (Wyatt et al., 2021) may have resulted in enhanced primary productivity in the near-shore regions. This process consumed nutrients from surface waters, and resulted in an excess of fluvial-derived dTMs (especially dCu) with respect to P in S-AC and S-BC compared to other surface waters.

4.2. Water masses, nutrient and dTM distributions at depths > 500 m along transect GA10

The similarities in the distributions of dTMs (Fig. 3) and water mass fractions (Fig. 1) indicated that water mass mixing played a key role in determining dTM concentrations and their relationships with nutrients at depths > 500 m. Endmember dTM concentrations of each water mass were estimated from relationships with significant correlation coefficients and low uncertainties (Table 3); e.g., correlation coefficients R^2 were > 0.9 for the final step to estimate the UCDW endmember. The relationships between dTMs and nutrients at depth, and in particular the observed kinks (e.g., at P of 2.3 μmol kg^{-1} for dCu-P and dZn-P relationships), and linear dTM-nutrient correlations at depths > 3000 m, could be reconstructed well by the simulated data (Fig. 6). Predicted dTM were comparable to the observed dTM concentrations. Almost all stations showed low residual (measured – reconstructed) dTM concentrations: dCd residual of −0.05–0.05 nmol kg^{-1} (root-mean-square error, rmse 0.052 nmol kg^{-1}), dCu residual of −0.2–0.2 nmol kg^{-1} (rmse 0.177 nmol kg^{-1}), dNi and dZn residuals of −0.5–0.5 nmol kg^{-1} (rmse 0.409 and 0.596 nmol kg^{-1}) (Fig. 8). The residuals are mostly < 10 % of the observed dTM concentrations (Fig. S9), consistent with the measurement uncertainties. These results demonstrate that our OMP method was robust in estimating the dTM endmember values of water masses. Distributions of dTMs and their relationships with nutrients in the South Atlantic Ocean at depths > 500 m can therefore largely be explained by the mixing of water masses without the need to involve local biogeochemical processes.

The difference between simulated and measured dissolved oxygen concentrations (O_2 deficit) can provide a measure of the degree of remineralization that locally occurred in the water column (Middag et al., 2018). Note that O_2 deficit is not the same as apparent oxygen utilization that represents O_2 consumption relative to atmospheric equilibrium. The O_2 deficit can also be estimated using the extended OMP approach assuming remineralization with Redfield ratio of ΔP: ΔN: ΔSi: ΔO_2 = 1: 16: 40: −170 (Anderson and Sarmiento, 1994; Karstensen and Tomczak, 1998). Both the classical and extended OMP generated O_2 deficits with similar ranges and distribution patterns (Fig. 8, Fig. S10). Specifically, the O_2 deficits estimated from classical OMP fall in a narrow range of between −14 and 36 μmol kg^{-1}, with most values ranging from −5 to 5 μmol kg^{-1} (Fig. 8). The O_2 deficits calculated from extended OMP mostly ranged from 0 to 50 μmol kg^{-1} (3rd quantile 10.8 μmol kg^{-1}) with an average of 7.49 ± 12.14 μmol kg^{-1}. If the calculated O_2 deficits were fully attributed to local remineralization of sinking phytoplankton cells, this process would produce maximum differences in P of 0.29 μmol kg^{-1}, TN of 4.71 μmol kg^{-1}, Si of 11.76 μmol kg^{-1}, dCd of 41 pmol kg^{-1}, dZn of 0.59 nmol kg^{-1}, dZn of 0.58 nmol kg^{-1}, and dCu of 0.15 nmol kg^{-1}, using the remineralization ratios of phytoplankton cells adopted from extended Redfield ratios ($\Delta P:\Delta O_2$ = 1: −170, $(Si_{40}N_{16}P_1)_{1000}Zn_{2.00}Cu_{0.51}Ni_{1.97}Cd_{0.14}$) (Fig. 7) (Anderson and Sarmiento, 1994; Ho et al., 2003; Twining and Baines, 2013). These differences in dTMs are minor relative to their measured ranges, suggesting that dTM distributions at depth were minimally affected by local remineralization process. Furthermore, relatively large O_2 deficits were identified at intermediate depths of 200–1000 m from classical OMP and 1000–2000 m from extended OMP (since remineralization should occur at shallower depths, this result indicates that O_2 deficits can be better explained by classical OMP), where positive residuals of nutrients and dTMs were not consistently observed (Fig. 8, Fig. S10). Therefore, the low O_2 deficits observed at intermediate depths could be a result of uncertainties associated with O_2 measurements and modeling, rather than associated with locally occurring remineralization. Our findings concur with Middag et al., (2018,2019,2020) who reported that regional remineralization at depth >500 m played a minor role in setting the distributions of dCd, dNi, and dZn in the Atlantic Ocean along the GEOTRACES GA02 transect.

Negative dTM residuals were not observed at stations #20 and #21

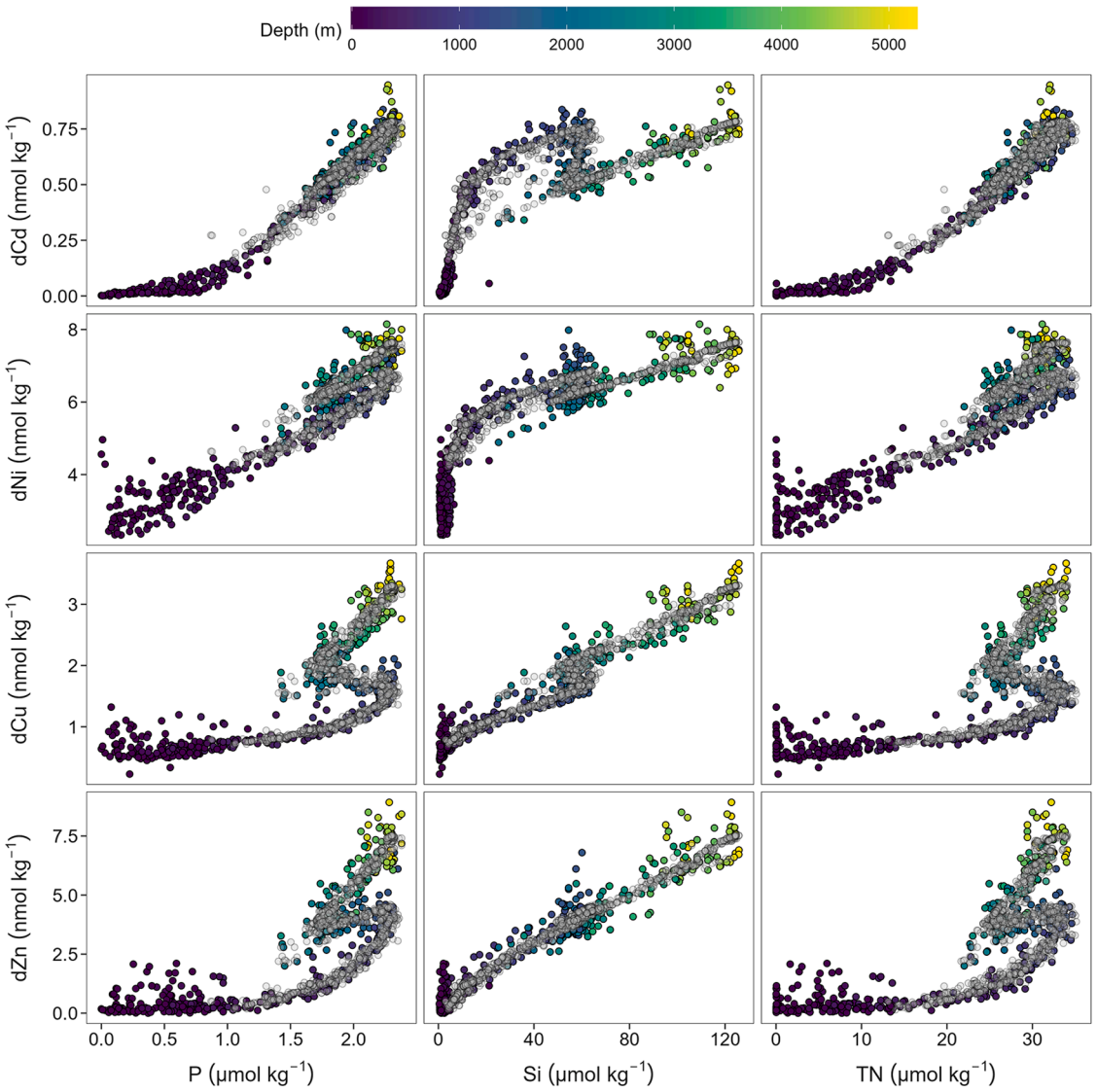

Fig. 6. Relationships between nutrients and nutrient-type dissolved trace metals (dCd, dCu, dNi, and dZn) along the GA10 transect in the South Atlantic Ocean. Gray points represent reconstructed data (only for depth > 200 m and temperature < 10 °C) by direct multiplication of water mass fractions with their endmember compositions.

at depths of ~ 2000–3200 m (Fig. 8). This region is characterized by the highest NADW fractions (70–96 %), consistent with the major pathway along the western side of the South Atlantic Ocean (Garzoli et al., 2015; Stramma and England, 1999). Therefore, the observed low nutrient and dTM levels at stations #20 and #21 (Fig. 3) were caused by a higher contribution of NADW which has lower endmember nutrient and dTM concentrations than AABW and UCDW (Table 3).

The elevated dTM concentrations on the eastern side (stations #2, #5, and #6) of the GA10 transect (Fig. 3) were accompanied by relatively large positive residuals of dCu (>0.2 nmol kg^{-1}), dNi (>0.5 nmol kg^{-1}), and dZn (>0.5 nmol kg^{-1}) (Fig. 8), with relative residuals of > 10 % (Fig. S9). The largest dTM residuals were identified at station #2, followed by intermediate waters of station #5 and bottom waters of station #6 (all collected during D357). D357 only sampled the eastern side of the transect, one year prior to JC068. Hence, the observed dTM discrepancies were probably attributed to spatial and/or temporal variations (Wyatt et al., 2021) in the dTM concentrations of dynamic water masses. Specifically, the positive dTM residuals near the African coast can be related to the occurrence of offshore nepheloid layers (Inthorn et al., 2006), which delivered dTMs from the Agulhas Bank sediments with reduced oxygen levels (Boye et al., 2012; Chapman and Shannon, 1987; Wyatt et al., 2021). Elevated dissolved and labile particulate Co, Fe, Mn, and Pb have been reported close to South Africa, related to the metal-enriched Agulhas current and South African continental shelf (Boye et al., 2012; Chever et al., 2010; Paul et al., 2015). Bottom water enrichments of dTMs on the eastern side of the transect were attributed to spatial variations in AABW. At depths > 2500 m, similar relationships between Θ and nutrients and dCd (Fig. S11) were observed for both D357 and JC068. In contrast, samples from cruise D357 showed moderately larger y-intercepts for the dCu-Θ, dNi-Θ, and dZn-Θ relationships (i.e., higher endmember dTM concentrations of AABW) compared to JC068 (Fig. S11). Therefore, AABW in the east showed higher dTM concentrations (positive dTM residuals) but similar nutrient levels than on the western side, possibly reflecting the different transport lengths and pathways of AABW (Solodoch et al., 2022).

A strong pTM enrichment was observed in bottom waters of the Argentine Basin (Fig. 5). All total and labile pTMs showed significant correlations with total pAl and pP (Fig. 7), demonstrating that these pTMs were originated from a similar source, probably seafloor sediments. The total pNi:pAl ratio is close to the UCC value (Rudnick and Gao, 2003), suggesting that pNi was mainly supplied by lithogenic particles. The total pCd:pAl, pCu:pAl, and pZn:pAl ratios were much

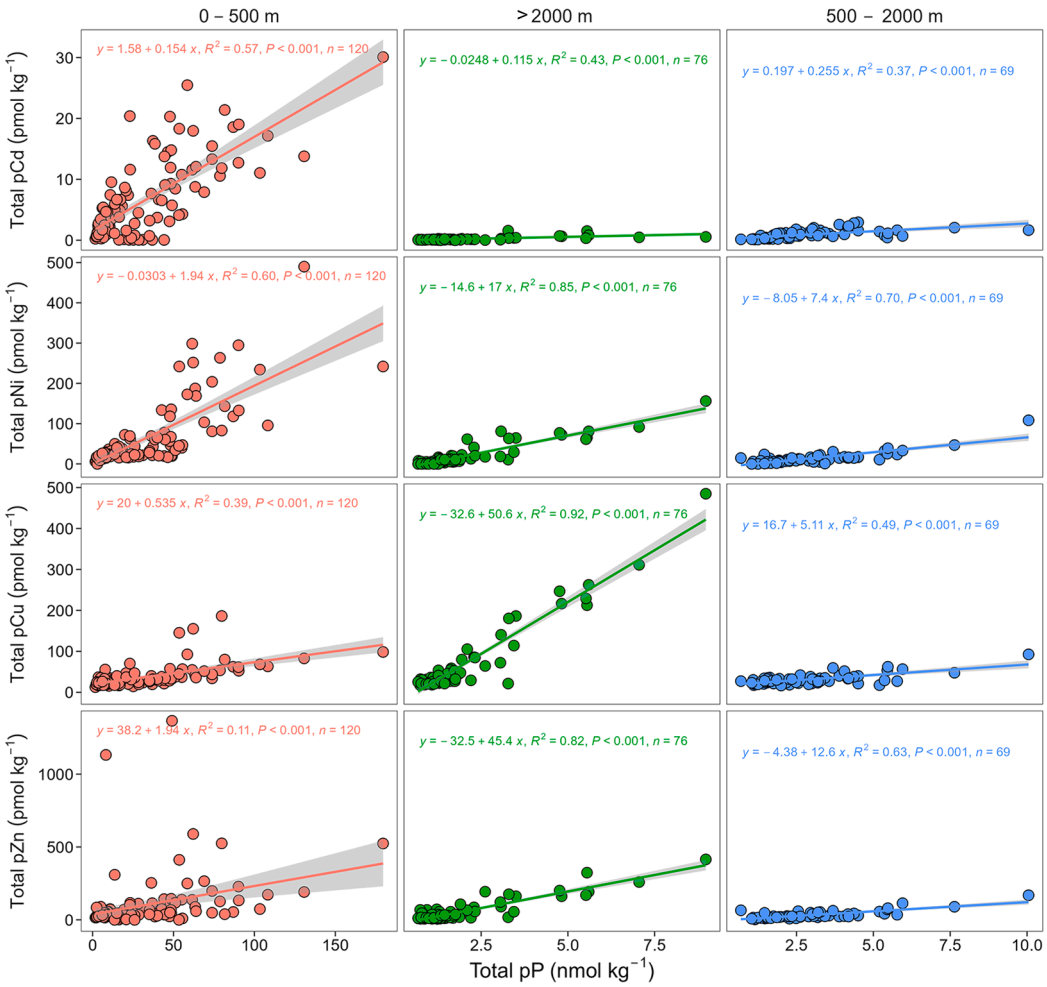

Fig. 7. Correlations between total particulate Cd (Total pCd), Ni (Total pNi), Cu (Total pCu), Zn (Total pZn) and P (Total pP) along the GA10 transect in the South Atlantic Ocean. Linear regression models were applied to samples with depths < 500 m, > 2000 m, and 500–2000 m, respectively.

higher than the UCC ratios, indicating an additional source of pTMs to the sediments, probably sunken phytoplankton debris and/or marine authigenic clays. Benthic inputs via reductive dissolution may have elevated the dTMs concentrations in bottom waters in the Argentine Basin (Fig. 3, Fig. S11). Nevertheless, this process does not produce pronounced changes in AABW endmember characteristics, and no significant dTM residuals were observed in the Argentine Basin (Fig. 8, Fig. S9). In addition, direct hydrothermal inputs of dTMs and pTMs on the Mid-Atlantic Ridge were not observed in this study. This finding is consistent with previous work that hydrothermal inputs posed little influence on the distributions of dCd and dZn in the South Atlantic Ocean (Wyatt et al., 2014; Xie et al., 2015).

4.3. *Impacts of Southern Ocean processes on the dTM-nutrient relationships in waters of Antarctic origin*

Water mass mixing has been invoked to explain the distributions of lead (Pb) (Schlosser et al., 2019) and dissolved gaseous mercury (Bratkič et al., 2016; Živković et al., 2022) along the GA10 transect. Our findings further demonstrated that the distributions of nutrient-type dTMs and nutrients at depth were determined by mixing of Antarctic waters and NADW that are driven by the global thermohaline circulation. During the transport of water masses from their formation regions to the study region, their nutrient-dTM stoichiometries are determined by the preformed concentrations, remineralization, sinking of particles, and/or external sources. AABW in the Atlantic sector is formed along the continental margins of the Weddel Sea, and is a mixture of dense continental shelf water and offshore UCDW (Talley, 2011). The preformed nutrient and dTM concentrations of AABW, represented by waters at depths > 3000 m in the Weddell Gyre (WG), are almost identical to the endmember values of AABW in the South Atlantic (Cloete et al., 2019; Croot et al., 2011; GEOTRACES IDP 2021) (Table 4). UCDW is a dominant water mass that supplies nutrients and dTMs to the surface waters of the Antarctic Zone (AZ) and WG (Morozov et al., 2021). If we take surface waters in the WG or waters with $O_2 < 180$ μmol kg^{-1} and temperature of 1.5–2.5 °C in the AZ and WG (Talley, 2011) to represent the original UCDW, the maximum differences in nutrient and dTM concentrations between UCDW in the South Atlantic and preformed UCDW is minor, showing values of P 0.51 ± 0.13 μmol kg^{-1}, TN 8.3 ± 2 μmol kg^{-1}, Si 0.8 ± 5.8 μmol kg^{-1}, dCd 129 ± 199 pmol kg^{-1}, dCu 0.24 ± 0.34 nmol kg^{-1}, and dZn 2.03 ± 0.87 nmol kg^{-1} (Table 4). The subduction of surface waters in the Polar Front Zone (PFZ) forms AAIW (Rintoul et al., 2001; Sloyan and Rintoul, 2001). Surface waters in the AZ (the original AAIW before subduction) and endmember AAIW in the South Atlantic also showed comparable nutrient and dTM concentrations, e.g., with differences in dCd of 53 ± 150 pmol kg^{-1}, dCu of −0.1 ± 0.21 nmol kg^{-1}, and dZn of −0.8 ± 0.64 nmol kg^{-1} (Table 4). All these results indicate that the nutrient-dTM stoichiometries of AAIW, UCDW, and AABW are largely set in their formation regions in the Southern Ocean, while remineralization, scavenging removal and external sources played negligible roles during their lateral transport to the South Atlantic.

The differences in nutrient and dTM endmember concentrations between UCDW, AAIW, and SACW are controlled by surface phytoplankton activities in the Southern Ocean. In surface waters of large

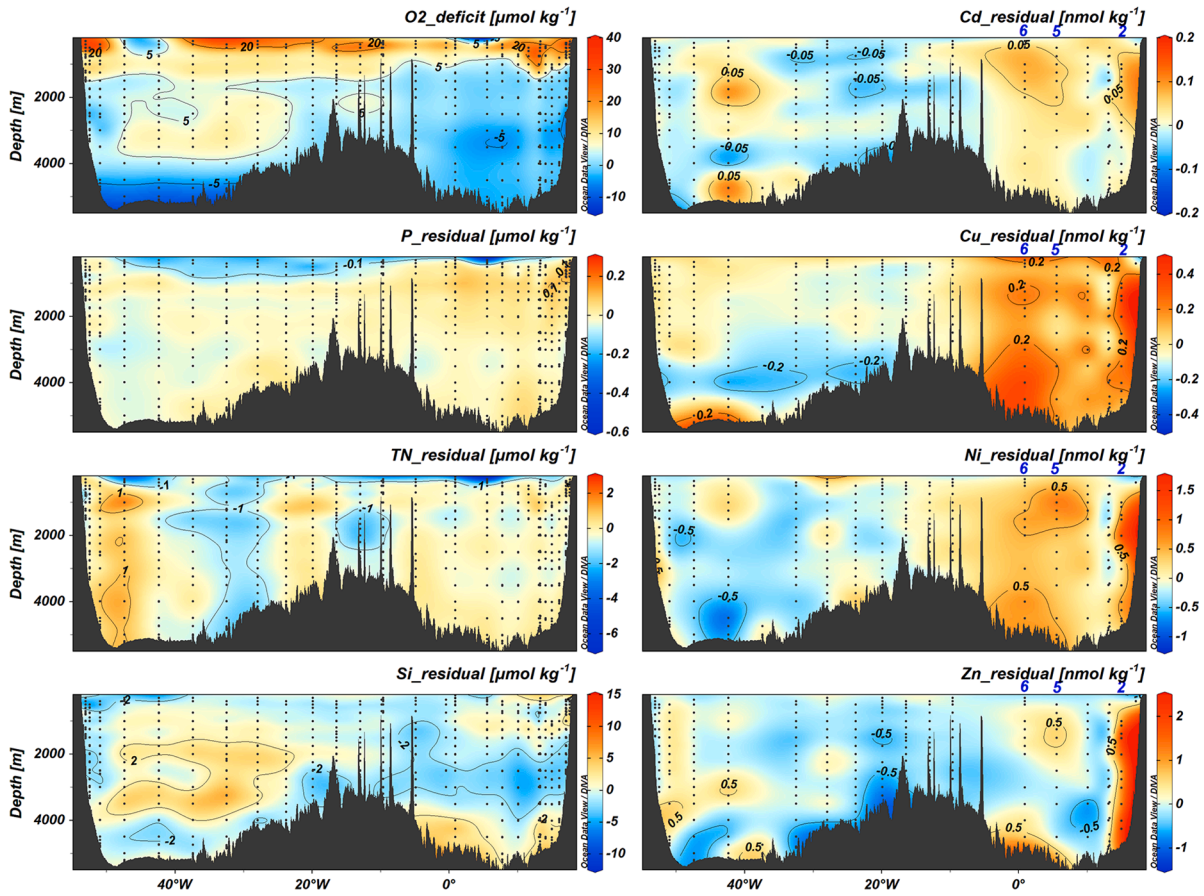

Fig. 8. Residuals (measured – reconstructed) of oxygen (O_2), nutrients (phosphate [P], nitrate+nitrite [TN], and silicic acid [Si]), and dissolved trace metals (Cd, Cu, Ni, and Zn) along transect GA10. Stations #2, #5, and #6 with positive residuals of dTMs are labeled in blue.

parts of the Southern Ocean, phytoplankton communities are dominated by diatoms (Armbrust, 2009; Browning et al., 2014a). Under the prevailing condition of Fe limitation in the Southern Ocean (Moore et al., 2013), diatoms over-silicify with enhanced removal of Si, Zn, and Cu from surface waters relative to P and TN (Franck et al., 2000; Roshan et al., 2018; Sarmiento et al., 2004), leading to discrepancies in Si:P, dZn:P, and dCu:P ratios between UCDW and AAIW. This process is demonstrated by the correlations between dTMs and nutrients in surface waters (depths < 100 m) of the WG (Fig. S12). The inferred dCu-dZn-Si-P uptake stoichiometries (Cu:Zn:Si:P = 1.15 ± 0.53: 6.97 ± 1.34: 72.9 ± 3.9 × 10^3:1000) are generally consistent with the differences between UCDW and AAIW endmembers (ΔP = 0.33 ± 0.07 μmol kg^{-1}, ΔSi = 51.9 ± 1.3 μmol kg^{-1}, ΔdCu = 0.71 ± 0.07 nmol kg^{-1}, and ΔdZn = 3.29 ± 0.25 nmol kg^{-1}. Table 3). Likewise, the continued phytoplankton uptake in the PFZ and SAZ, with much lower Cu:P (0.17 ± 0.39 × 10^{-3}), Zn:P (0.17 ± 0.39 × 10^{-3}), and Si:P (11.2 ± 1.1) ratios (Fig. S12), generated surface waters strongly depleted in nutrients and dTMs. These surface waters travel north into the Sub-Antarctic Zone (SAZ) and subduct to form Sub-Antarctic Mode Water (SAMW), which makes an important contribution to SACW (Liu and Tanhua, 2021; Stramma and England, 1999). As a result, SACW showed the lowest Si/P, dZn/P, and dCu/P ratios, followed by AAIW and UCDW (Fig. 9, Table 3). The drastic changes in uptake stoichiometry in the Southern Ocean are ascribed to a shift from a diatom-dominated phytoplankton community in the AZ to a mixed community including coccolithophores in the SAZ (Nissen et al., 2021), probably in response to the decrease in Si concentrations in surface waters.

Linear relationships were observed for dCd-P and dNi-P at depth (Fig. 6). The linear dCd-P relationship is ascribed to the consistent dCd:P ratios for the various water masses (Fig. 9). For instance, the NADW-AABW and SACW-AAIW-UCDW-AABW mixing lines have similar equations of y = 0.511 *x −0.394 and y = 0.582*x-0.562, respectively. These equations are also almost identical to the deep water dCd-P relationships along the GA02 transect (Middag et al., 2018), indicating that the dCd-P relationship in the Atlantic Ocean was spatially and temporally constant. Nevertheless, AABW and UCDW (~0.34 × 10^{-3}) illustrated higher spot dCd/P ratios than AAIW (0.283 × 10^{-3}), NADW (0.235 × 10^{-3}), and SACW (0.116 × 10^{-3}). The dCd/P ratio of NADW was probably inherited from the remineralization Cd:P ratio (0.2–0.3 × 10^{-3}) of phytoplankton cells in the nutrient-poor high latitude North Atlantic (Quay et al., 2015; Roshan and Wu, 2015b). In the Southern Ocean, the high nutrient supply to surface waters via upwelling and prevailing micro-nutrient (Fe, Zn, Mn) limitation (Browning et al., 2021; Hawco et al., 2022), resulted in enhanced Cd uptake relative to P by phytoplankton (Baars et al., 2014; Cullen, 2006; Sunda and Huntsman, 2000). This process is consistent with the elevated uptake Cd:P ratios (0.74–0.83 × 10^{-3}) in the Southern Ocean (Fig. S12), which eventually set the dCd/P stoichiometries of UCDW, AAIW, and SACW (Fig. 9). Therefore, the linear dCd-P relationship in the South Atlantic at depth was the consequence of mixing of Antarctic waters and NADW with distinctive uptake/remineralization ratios. Hence, assessments of local process in the source regions of water masses are required as they imprint on the subsequent mixing processes during large scale ocean circulation and will determine downstream biogeochemical cycling of dTMs.

The relationship between reconstructed dNi and P showed twisted curves (Fig. 6), consistent with the depth-dependent dNi-P relations at each station (Fig. S13). Direct calculation of the uptake Ni:P ratios in the Southern Ocean is not possible due to a lack of dNi data. Instead, the uptake stoichiometry of Ni:P by phytoplankton is estimated as 2.44 ± 0.33 × 10^{-3} by contrasting the SACW and UCDW endmember

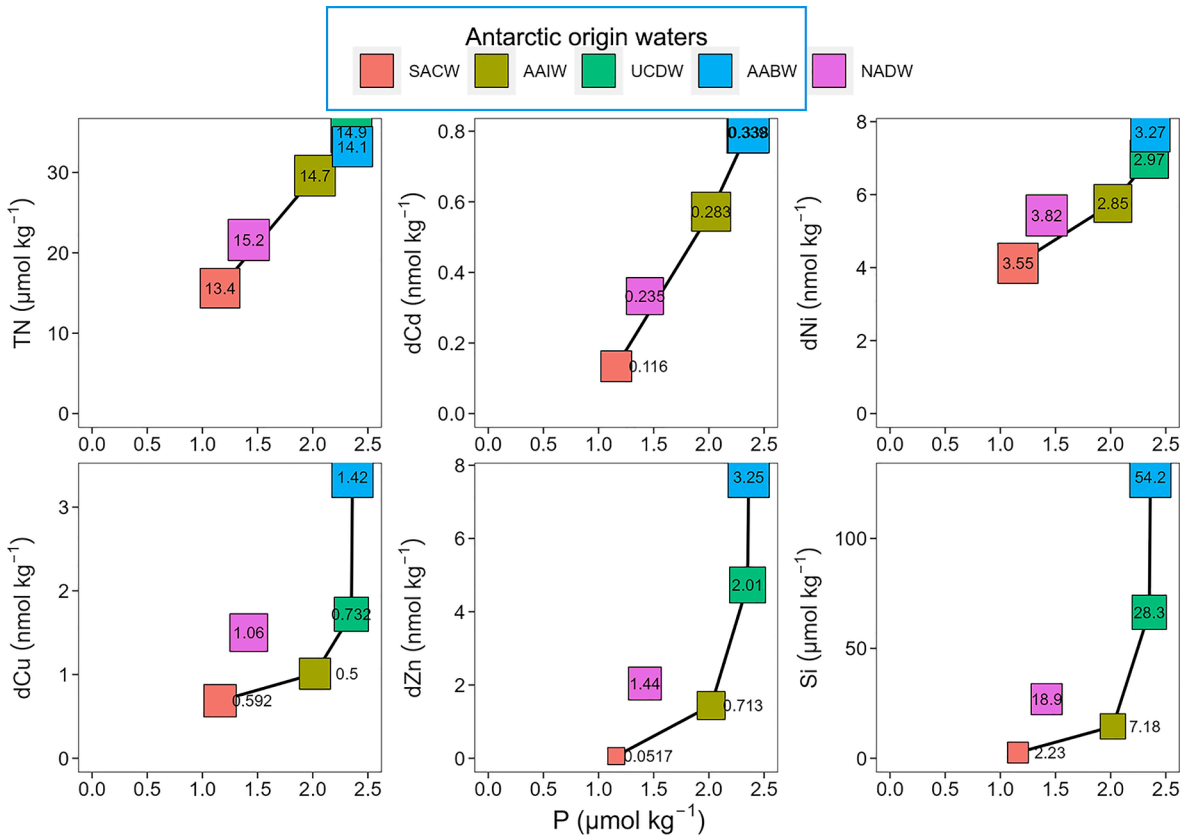

Fig. 9. Relationships between endmember nitrate+nitrite (TN), silicic acid (Si), nutrient-like dissolved trace metals (dTMs, dCd, dCu, dNi, and dZn) and phosphate (P) of water masses (South Atlantic Central Water [SACW], Antarctic Intermediate Water [AAIW], Upper Circumpolar Deep Water [UCDW], North Atlantic Deep Water [NADW], and Antarctic Bottom Water [AABW]) in the South Atlantic Ocean. The numbers in squares represent the ratios between TN, Si, dTMs, and P with units as per the coordinates.

concentrations (Table 3). This ratio is essentially close to the dNi:P relationships of AABW-NADW and NADW-AAIW mixing (Middag et al., 2020). This suggests that the overall linear dNi-P relationship in the South Atlantic is determined by mixing of water masses with different spot dNi/P ratios (Fig. 9), and driven by the similarities between Ni:P uptake ratios in the Southern Ocean and ΔdNi:ΔP of AAIW-NADW-AABW. Variations in cellular Ni:P with phytoplankton species (e.g., highest Ni:P ratios in nitrogen-fixing cyanobacteria; Twining and Baines, 2013), higher Ni requirements for diatoms, and 50 % cellular Ni quota in diatom opal (Twining et al., 2012) are not observable in this study.

Unlike the other dTMs, a significant portion of dNi in seawater remains in surface waters during phytoplankton growth, possibly due to strong organic ligand complexation and/or slow depletion of Ni by biological uptake (Boiteau et al., 2016; John et al., 2022; Mackey et al., 2002), and/or limited membrane protein space for dNi uptake (Price and Morel, 1991). The residual dNi relative to P in the South Atlantic, estimated from the linear dNi-P correlation in top waters, was ~ 2.5 nmol kg^{-1} (Fig. S3). This value is somewhat larger than the residual dNi in the North Atlantic (~1.7 nmol kg^{-1}), and possibly related to higher nitrogen fixation rates in the North Atlantic Subtropical Gyre (NASTG) that would remove Ni (Benavides and Voss, 2015; Cloete et al., 2019).

4.4. *dTM-nutrient stoichiometries fixed at high latitude oceans*

The Southern Ocean is a highly dynamic region. Vigorous upwelling, mixing, and subduction of water masses in the AZ and PFZ sustain primary productivity in surface waters and generate Antarctic origin waters (AAIW, AABW, and UCDW) with different geochemical signatures (Rintoul et al., 2001; Sloyan and Rintoul, 2001). During thermohaline circulation, these Antarctic origin waters are transported eastward with the ACC and northward into adjacent subtropical gyres, e.g., the SASTG, Indian Ocean STG, and South Pacific STG. The influence of the AAIW is still distinguishable at intermediate depth at latitude < 20°N in the Atlantic Ocean and < ~ 10°N in the Pacific Ocean. The cold and dense AABW occupies the bottom water of all ocean basins that have a connection to the Southern Ocean (Talley, 2011). The physical and chemical properties of water masses evolve during their lateral transport and mixing with other water masses. However, our results indicate that the endmember characteristics of Antarctic origin waters have only changed slightly during their lateral transport into the subtropical gyres (Fig. 10). The predicted nutrient and dTM endmember levels of AAIW, UCDW, AABW, and NADW in this study are comparable to those reported across the Atlantic Ocean (Table 3) (Liu et al., 2022b; Middag et al., 2018, 2019, 2020). The endmember dTM concentrations of AAIW and AABW calculated for the SASTG are statistically indistinguishable from those in the NASTG (Fig. 10). For instance, the dCd, dNi, and dZn endmember concentrations of AAIW remain at 0.53–0.57 nmol kg^{-1}, 5.25–5.76 nmol kg^{-1}, and 1.16–1.44 nmol kg^{-1} at GEOTRACES transects GA10 and GA02. More importantly, the nutrient and dTM concentration ranges of AABW were similar for various GEOTRACES transects (GA10: 40°S South Atlantic; GA02: across the west Atlantic; GA02-N: GA02 at latitudes > 0°N; GA03: North Atlantic at latitudes 15–40°N; GA08: Southwest Atlantic at latitudes 28.8–3°S) (Table 3). All these results demonstrate that the dTM-nutrient stoichiometries of Antarctic-derived waters have been set in the Southern Ocean.

In addition, our calculated dTM concentrations for NADW resembled those predicted for the North Atlantic Ocean (latitudes > 0°N) (Table 3).

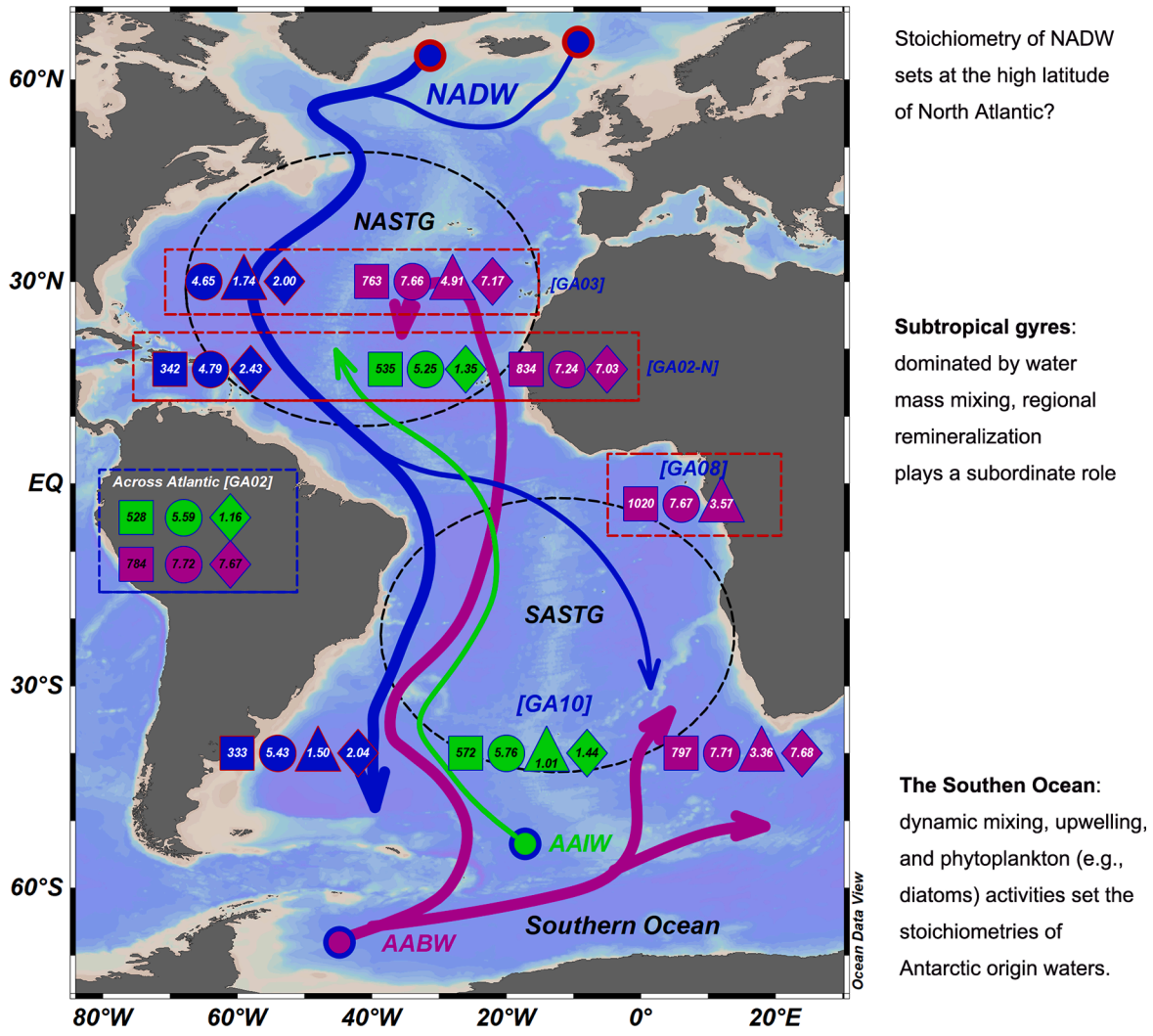

Fig. 10. Schematic showing the variations in endmember dTM concentrations of Antarctic origin waters (Antarctic Intermediate Water [AAIW, in green] and Antarctic Bottom Water [AABW, purple]) and Nordic origin water (North Atlantic Deep Water [NADW, blue]) in the Atlantic Ocean. The rimmed dots indicate the formation regions of the water masses. Endmember dTM concentrations of water masses (GA10) in the South Atlantic Subtropical Gyre (SASTG) were derived from this study, while those in the North Atlantic Subtropical Gyre (NASTG) were estimated from GA02, GA03, and GA08 transects using their established relationship between dTMs and nutrients. The colors of symbols with endmember values (dCd: squares, dNi: circles, dCu: triangles, dZn: diamonds. Units are in pmol kg^{-1} for dCd and nmol kg^{-1} for dNi, dCu, and dZn) match the colors of water masses. For details of the source data see Table 3.

The endmember dCd, dCu, and dZn concentrations of NADW remain at 0.33–0.34 nmol kg^{-1}, 1.50–1.74 nmol kg^{-1}, and 2.00–2.43 nmol kg^{-1} across the assessed regions from the NASTG to the SASTG. The calculated endmember dNi concentrations of NADW are higher along the transect GA10 compared to GA02, but still match those along the GA03 transect within uncertainties. The NADW is composed of various different source waters, including Denmark Strait Overflow Water, Labrador Sea Water, and Iceland-Scotland Overflow Water (van Aken, 2000). As we lack data on the specific source regions of NADW, when and where the nutrient-dTM stoichiometry of NADW was fixed is unknown. Our results indicate that the characteristics of NADW are relatively constant during transport from > 0°N to 40°S in the Atlantic Ocean. Regional remineralization in the Atlantic, therefore, plays a subordinate role in setting the concentrations of nutrients and dTMs in the intermediate and deep waters of the North and South Atlantic Ocean. External inputs from sediments and rivers may be an important source of dTMs at regional scales (Liu et al., 2022b; Roshan and Wu, 2015a) but are not a dominant factor in controlling the basin-scale relationships between nutrient-type dTM and nutrient in the Atlantic Ocean.

5. Conclusions

The distributions of nutrients and nutrient-type dTMs and their relationships along the GA10 transect in the South Atlantic Ocean were closely related to the circulation system of the South Atlantic Subtropical Gyre. Nutrient and dTM concentrations in surface waters were generally determined by phytoplankton uptake. Fluvial materials from e.g. the Rio de la Plata were carried by coastal currents like the Brazil Current, supplied TMs in both dissolved and particulate phases to nearshore regions and stimulated enhanced primary productivity. This process, in turn, framed the relationships between dTMs and nutrients in adjacent surface waters.

The observed nutrient and dTM distributions at depth could be reconstructed by OMP analysis, showing low residuals between observed and simulated values. Therefore, dTM profiles and their relationships with nutrients in the South Atlantic can be resolved by the mixing of waters of Antarctic origin (AAIW, AABW, UCDW) and North Atlantic waters (NADW), without the need to invoke local remineralization. Diatom activities in the Southern Ocean played an essential role

in setting the elemental stoichiometries of Antarctic waters. The end-member characteristics of Antarctic origin waters and NADW changed only slightly across the Atlantic Ocean, demonstrating that the properties of these water masses were largely fixed in their formation regions. Hence, high latitude oceans (e.g., Southern Ocean and Labrador Sea) are key regions to set the stoichiometries of nutrients and dTMs in low latitude oceans via thermohaline circulation. Considering that high latitude oceans are highly dynamic and susceptible to environmental stress, climate change may affect the future phytoplankton communities in the Southern Ocean and consequently shape the supply of nutrients and micro-nutrients to low latitude waters. As the main return path of nutrients occurs in the Southern Ocean by upwelling and winter mixing, this process can potentially have consequences for primary production and biogeochemical cycles in the global ocean.

Data availability

Data are availabile through GEOTRACES Intermediate Data Product at https://geotraces.webodv.awi.de/IDP2021.

Declaration of competing interest

The authors declare that they have no known competing financial interests or personal relationships that could have appeared to influence the work reported in this paper.

Acknowledgments

The authors thank the captains and crew of *RRS Discovery* and *RRS James Cook*. We thank the chief scientist Gideon Henderson and other participants of both cruises for their on-board work, and Christian Schlosser for trace metal analysis. The research was supported by UK Natural Environment Research Council (NE/H00475/1 – UKGEOTRACES). The International GEOTRACES Programme is possible in part thanks to the support from the U.S. National Science Foundation (Grant OCE-1840868) to the Scientific Committee on Oceanic Research (SCOR).

Appendix A. Supplementary material

The supplementary material includes a supplementary table showing the processing blanks (Table S1), supplementary figures showing the property-property plots of water masses (Fig. S1), uncertainties of water mass analysis (Fig. S2), comparison in data quality (Fig. S3), correlations among dissolved and particulate trace metals and nutrients (Figs. S4, S5, S6, S7, S11), surface distributions of dissolved trace metals and fluorescence along the transect (Fig. S8), section profiles of relative residuals (Fig. S9) and O_2 deficits (Fig. S10) from water mass analysis, variations of dissolved trace metals and nutrients in the Southern Ocean (Fig. S12), and relationships between dissolved nickel and phosphate in the South Atlantic Ocean (Fig. S13). Supplementary material to this article can be found online at https://doi.org/10.1016/j.gca.2024.01.001.

References

Anderson, L.A., Sarmiento, J.L., 1994. Redfield ratios of remineralization determined by nutrient data analysis. Glob. Biogeochem. Cycles 8, 65–80.
Aphalo, P.J., 2022. ggpmisc: Miscellaneous Extensions to "ggplot2".
Archer, C., Vance, D., Milne, A., Lohan, M.C., 2020. The oceanic biogeochemistry of nickel and its isotopes: new data from the South Atlantic and the Southern Ocean biogeochemical divide. Earth Planet. Sci. Lett. 535, 116118.
Arhan, M., Mercier, H., Park, Y.-H., 2003. On the deep water circulation of the eastern South Atlantic Ocean. Deep Sea Res. Part Oceanogr. Res. Pap. 50, 889–916.
Armbrust, E.V., 2009. The life of diatoms in the world's oceans. Nature 459, 185–192.
Baars, O., Abouchami, W., Galer, S.J.G., Boye, M., Croot, P.L., 2014. Dissolved cadmium in the Southern Ocean: distribution, speciation, and relation to phosphate. Limnol. Oceanogr. 59, 385–399.
Becker, S., Aoyama, M., Woodward, E.M.S., Bakker, K., Coverly, S., Mahaffey, C., Tanhua, T., 2020. GO-SHIP repeat hydrography nutrient manual: the precise and accurate determination of dissolved inorganic nutrients in seawater, using continuous flow analysis methods. Front. Mar. Sci. 7, 581790.
Benavides, M., Voss, M., 2015. Five decades of N2 fixation research in the North Atlantic Ocean. Front. Mar. Sci. 2, 40.
Berger, C.J.M., Lippiatt, S.M., Lawrence, M.G., Bruland, K.W., 2008. Application of a chemical leach technique for estimating labile particulate aluminum, iron, and manganese in the Columbia River plume and coastal waters off Oregon and Washington. J. Geophys. Res. Oceans 113, C00B01.
Boiteau, R.M., Till, C.P., Ruacho, A., Bundy, R.M., Hawco, N.J., McKenna, A.M., Barbeau, K.A., Bruland, K.W., Saito, M.A., Repeta, D.J., 2016. Structural characterization of natural nickel and copper binding ligands along the US GEOTRACES eastern Pacific zonal transect. Front. Mar. Sci. 3, 243.
Boye, M., Wake, B.D., Lopez Garcia, P., Bown, J., Baker, A.R., Achterberg, E.P., 2012. Distributions of dissolved trace metals (Cd, Cu, Mn, Pb, Ag) in the southeastern Atlantic and the Southern Ocean. Biogeosciences 9, 3231–3246.
Boyle, E.A., 1988. Cadmium: chemical tracer of Deepwater paleoceanography. Paleoceanography 3, 471–489.
Bratkič, A., Vahčič, M., Kotnik, J., Obu Vazner, K., Begu, E., Woodward, E.M.S., Horvat, M., 2016. Mercury presence and speciation in the South Atlantic Ocean along the 40°S transect. Glob. Biogeochem. Cycles 30, 105–119.
Browning, T.J., Bouman, H.A., Henderson, G.M., Mather, T.A., Pyle, D.M., Schlosser, C., Woodward, E.M.S., Moore, C.M., 2014a. Strong responses of Southern Ocean phytoplankton communities to volcanic ash. Geophys. Res. Lett. 41, 2851–2857.
Browning, T.J., Bouman, H.A., Moore, C.M., Schlosser, C., Tarran, G.A., Woodward, E.M.S., Henderson, G.M., 2014b. Nutrient regimes control phytoplankton ecophysiology in the South Atlantic. Biogeosciences 11, 463–479.
Browning, T.J., Achterberg, E.P., Engel, A., Mawji, E., 2021. Manganese co-limitation of phytoplankton growth and major nutrient drawdown in the Southern Ocean. Nat. Commun. 12, 884.
Bruland, K.W., Knauer, G.A., Martin, J.H., 1978. Zinc in north-East Pacific water. Nature 271, 741–743.
Bruland, K.W., Middag, R., Lohan, M.C., 2014. Controls of trace metals in seawater. Treatise Geochem. 19–51.
Chance, R., Jickells, T.D., Baker, A.R., 2015. Atmospheric trace metal concentrations, solubility and deposition fluxes in remote marine air over the south-East Atlantic. Mar. Chem. Biogeochem. Trace Elements Isotopes 177, 45–56.
Chapman, P., Shannon, L.V., 1987. Seasonality in the oxygen minimum layers at the extremities of the Benguela system. South Afr. J. Mar. Sci. 5, 85–94.
Chen, X.-G., Krisch, S., Al-Hashem, A., Hopwood, M.J., Rutgers van der Loeff, M.M., Huhn, O., Lodeiro, P., Steffens, T., Achterberg, E.P., 2022. Dissolved, labile, and total particulate trace metal dynamics on the Northeast Greenland shelf. Glob. Biogeochem. Cycles 36, e2022GB007528.
Chen, X.-G., Rusiecka, D., Gledhill, M., Milne, A., Annett, A.L., Birchill, A.J., Lohan, M.C., Ussher, S., Woodward, E.M.S., Achterberg, E.P., 2023. Ocean circulation and biological processes drive seasonal variations of dissolved Al, Cd, Ni, Cu, and Zn on the Northeast Atlantic continental margin. Mar. Chem. 252, 104246.
Chever, F., Bucciarelli, E., Sarthou, G., Speich, S., Arhan, M., Penven, P., Tagliabue, A., 2010. Physical speciation of iron in the Atlantic sector of the Southern Ocean along a transect from the subtropical domain to the Weddell Sea Gyre. J. Geophys. Res. Oceans 115, C10059.
Cloete, R., Loock, J.C., Mtshali, T., Fietz, S., Roychoudhury, A.N., 2019. Winter and summer distributions of copper, zinc and nickel along the international GEOTRACES section GIPY05: insights into deep winter mixing. Chem. Geol. 511, 342–357.
Croot, P.L., Baars, O., Streu, P., 2011. The distribution of dissolved zinc in the Atlantic sector of the Southern Ocean. Deep Sea Res. Part II Top. Stud. Oceanogr. 58, 2707–2719.
Cullen, J.T., 2006. On the nonlinear relationship between dissolved cadmium and phosphate in the modern global ocean: Could chronic iron limitation of phytoplankton growth cause the kink? Limnol. Oceanogr. 51, 1369–1380.
Cutter, G., Casciotti, K., Croot, P., Geibert, W., Heimbürger, L.-E., Lohan, M., Planquette, H., van de Flierdt, T., 2017. Sampling and Sample-handling Protocols for GEOTRACES Cruises. Version 3, August 2017. GEOTRACES Stand. Intercalibration Comm.
Dupont, C.L., Buck, K.N., Palenik, B., Barbeau, K., 2010. Nickel utilization in phytoplankton assemblages from contrasting oceanic regimes. Deep Sea Res. Part Oceanogr. Res. Pap. 57, 553–566.
Evans, N., Schroeder, I.D., Pozo Buil, M., Jacox, M.G., Bograd, S.J., 2020. Drivers of subsurface deoxygenation in the Southern California current system. Geophys. Res. Lett. 47, e2020GL089274.
Franck, V., Brzezinski, M.A., Coale, K.H., Nelson, D.M., 2000. Iron and silicic acid concentrations regulate Si uptake north and south of the polar frontal zone in the Pacific sector of the Southern Ocean. Deep Sea Res. Part II Top. Stud. Oceanogr. 47, 3315–3338.
Garzoli, S.L., Dong, S., Fine, R., Meinen, C.S., Perez, R.C., Schmid, C., van Sebille, E., Yao, Q., 2015. The fate of the deep Western boundary current in the South Atlantic. Deep Sea Res. Part Oceanogr. Res. Pap. 103, 125–136.

GEOTRACES Intermediate Data Product Group, 2021. The GEOTRACES Intermediate Data Product 2021 (IDP2021). NERC EDS Br. Oceanogr. Data Cent. NOC.
Gosnell, K.J., Landing, W.M., Milne, A., 2012. Fluorometric detection of total dissolved zinc in the southern Indian Ocean. Mar. Chem. 132, 68–76.
Hawco, N.J., Tagliabue, A., Twining, B.S., 2022. Manganese limitation of phytoplankton physiology and productivity in the Southern Ocean. Glob. Biogeochem. Cycles 36, e2022GB007382.
Ho, T.-Y., Quigg, A., Finkel, Z.V., Milligan, A.J., Wyman, K., Falkowski, P.G., Morel, F.M. M., 2003. The elemental composition of some marine Phytoplankton1. J. Phycol. 39, 1145–1159.
Homoky, W.B., Severmann, S., McManus, J., Berelson, W.M., Riedel, T.E., Statham, P.J., Mills, R.A., 2012. Dissolved oxygen and suspended particles regulate the benthic flux of iron from continental margins. Mar. Chem. 134, 59–70.
Horner, T.J., Lee, R.B.Y., Henderson, G.M., Rickaby, R.E.M., 2013. Nonspecific uptake and homeostasis drive the oceanic cadmium cycle. Proc. Natl. Acad. Sci. 110, 2500–2505.
Inthorn, M., Mohrholz, V., Zabel, M., 2006. Nepheloid layer distribution in the Benguela upwelling area offshore Namibia. Deep Sea Res. Part Oceanogr. Res. Pap. 53, 1423–1438.
Jacquot, J.E., Moffett, J.W., 2015. Copper distribution and speciation across the international GEOTRACES section GA03. Deep Sea Res. Part II Top. Stud. Oceanogr. 116, 187–207.
Jenkins, W.J., Smethie, W.M., Boyle, E.A., Cutter, G.A., 2015. Water mass analysis for the U.S. GEOTRACES (GA03) North Atlantic sections. Deep Sea Res. Part II Top. Stud. Oceanogr. 116, 6–20.
John, S.G., Kelly, R.L., Bian, X., Fu, F., Smith, M.I., Lanning, N.T., Liang, H., Pasquier, B., Seelen, E.A., Holzer, M., Wasylenki, L., Conway, T.M., Fitzsimmons, J.N., Hutchins, D.A., Yang, S.-C., 2022. The biogeochemical balance of oceanic nickel cycling. Nat. Geosci. 15, 1–7.
Karstensen, J., Tomczak, M., 1998. Age determination of mixed water masses using CFC and oxygen data. J. Geophys. Res. Oceans 103, 18599–18609.
La Fontaine, S., Quinn, J.M., Nakamoto, S.S., Page, M.D., Göhre, V., Moseley, J.L., Kropat, J., Merchant, S., 2002. Copper-dependent iron assimilation pathway in the model photosynthetic eukaryote Chlamydomonas reinhardtii. Eukaryot. Cell 1, 736–757.
Lane, T.W., Morel, F.M., 2000. A biological function for cadmium in marine diatoms. Proc. Natl. Acad. Sci. 97, 4627–4631.
Lane, T.W., Saito, M.A., George, G.N., Pickering, I.J., Prince, R.C., Morel, F.M.M., 2005. A cadmium enzyme from a marine diatom. Nature 435, 42.
Larqué, L., Maamaatuaiahutapu, K., Garçon, V., 1997. On the intermediate and deep water flows in the South Atlantic Ocean. J. Geophys. Res. Oceans 102, 12425–12440.
Little, S.H., Archer, C., Milne, A., Schlosser, C., Achterberg, E.P., Lohan, M.C., Vance, D., 2018. Paired dissolved and particulate phase Cu isotope distributions in the South Atlantic. Chem. Geol. 502, 29–43.
Liu, T., Krisch, S., Hopwood, M.J., Achterberg, E.P., Mutzberg, A., 2022a. Trace metal data from water samples during METEOR cruise M121. https://doi.org/10.1594/PANGAEA.947275.
Liu, T., Krisch, S., Xie, R.C., Hopwood, M.J., Dengler, M., Achterberg, E.P., 2022b. Sediment release in the Benguela upwelling system dominates trace metal input to the shelf and eastern South Atlantic Ocean. Glob. Biogeochem. Cycles 36, e2022GB007466.
Liu, M., Tanhua, T., 2021. Water masses in the Atlantic Ocean: characteristics and distributions. Ocean Sci. 17, 463–486.
Lohan, M.C., Tagliabue, A., 2018. Oceanic micronutrients: Trace metals that are essential for marine life. Elements 14, 385–390.
Lopez, J.S., Lee, L., Mackey, K.R., 2019. The toxicity of copper to Crocosphaera watsonii and other marine phytoplankton: a systematic review. Front. Mar. Sci. 5, 511.
Mackey, D.J., O'Sullivan, J.E., Watson, R.J., Dal Pont, G., 2002. Trace metals in the Western Pacific: temporal and spatial variability in the concentrations of Cd, Cu, Mn and Ni. Deep Sea Res. Part Oceanogr. Res. Pap. 49, 2241–2259.
Mahaffey, C., Reynolds, S., Davis, C.E., Lohan, M.C., 2014. Alkaline phosphatase activity in the subtropical ocean: insights from nutrient, dust and trace metal addition experiments. Front. Mar. Sci. 1, 73.
Middag, R., van Heuven, S.M.A.C., Bruland, K.W., de Baar, H.J.W., 2018. The relationship between cadmium and phosphate in the Atlantic Ocean unravelled. Earth Planet. Sci. Lett. 492, 79–88.
Middag, R., de Baar, H.J.W., Bruland, K.W., 2019. The relationships between dissolved zinc and major nutrients phosphate and silicate along the GEOTRACES GA02 transect in the West Atlantic Ocean. Glob. Biogeochem. Cycles 33, 63–84.
Middag, R., de Baar, H.J.W., Bruland, K.W., van Heuven, S.M.A.C., 2020. The distribution of nickel in the West-Atlantic Ocean, its relationship with phosphate and a comparison to cadmium and zinc. Front. Mar. Sci. 7, 105.
Milne, A., Schlosser, C., Wake, B.D., Achterberg, E.P., Chance, R., Baker, A.R., Forryan, A., Lohan, M.C., 2017. Particulate phases are key in controlling dissolved iron concentrations in the (sub)tropical North Atlantic. Geophys. Res. Lett. 44, 2377–2387.
Moore, C.M., Mills, M.M., Arrigo, K.R., Berman-Frank, I., Bopp, L., Boyd, P.W., Galbraith, E.D., Geider, R.J., Guieu, C., Jaccard, S.L., Jickells, T.D., La Roche, J., Lenton, T.M., Mahowald, N.M., Marañón, E., Marinov, I., Moore, J.K., Nakatsuka, T., Oschlies, A., Saito, M.A., Thingstad, T.F., Tsuda, A., Ulloa, O., 2013. Processes and patterns of oceanic nutrient limitation. Nat. Geosci. 6, 701–710.
Morel, F.M.M., Price, N.M., 2003. The biogeochemical cycles of trace metals in the oceans. Science 300, 944–947.
Morel, F.M.M., Reinfelder, J.R., Roberts, S.B., Chamberlain, C.P., Lee, J.G., Yee, D., 1994. Zinc and carbon co-limitation of marine phytoplankton. Nature 369, 740–742.
Morozov, E.G., Tarakanov, R.Y., Frey, D.I., 2021. Deep water masses of the south and North Atlantic. In: Morozov, E.G., Tarakanov, R.Y., Frey, D.I. (Eds.), Bottom Gravity Currents and Overflows in Deep Channels of the Atlantic Ocean: Observations, Analysis, and Modeling. Springer International Publishing, Cham, pp. 1–42.
Nissen, C., Gruber, N., Münnich, M., Vogt, M., 2021. Southern Ocean phytoplankton community structure as a gatekeeper for global nutrient biogeochemistry. Glob. Biogeochem. Cycles 35, e2021GB006991.
Ohnemus, D.C., Auro, M.E., Sherrell, R.M., Lagerström, M., Morton, P.L., Twining, B.S., Rauschenberg, S., Lam, P.J., 2014. Laboratory intercomparison of marine particulate digestions including Piranha: a novel chemical method for dissolution of polyethersulfone filters. Limnol. Oceanogr. Methods 12, 530–547.
Paul, M., van de Flierdt, T., Rehkämper, M., Khondoker, R., Weiss, D., Lohan, M.C., Homoky, W.B., 2015. Tracing the Agulhas leakage with lead isotopes. Geophys. Res. Lett. 42, 8515–8521.
Price, N.M., Morel, F.M.M., 1991. Colimitation of phytoplankton growth by nickel and nitrogen. Limnol. Oceanogr. 36, 1071–1077.
Quay, P., Cullen, J., Landing, W., Morton, P., 2015. Processes controlling the distributions of Cd and PO_4 in the ocean. Glob. Biogeochem. Cycles 29, 830–841.
Quay, P., Wu, J., 2015. Impact of end-member mixing on depth distributions of δ13C, cadmium and nutrients in the N. Atlantic Ocean. Deep Sea Res. Part II Top. Stud. Oceanogr. 116, 107–116.
Rapp, I., Schlosser, C., Rusiecka, D., Gledhill, M., Achterberg, E.P., 2017. Automated preconcentration of Fe, Zn, Cu, Ni, Cd, Pb, Co, and Mn in seawater with analysis using high-resolution sector field inductively-coupled plasma mass spectrometry. Anal. Chim. Acta 976, 1–13.
Rintoul, S.R., Hughes, C.W., Olbers, D., 2001. The Antarctic circumpolar current system. In: International Geophysics. Elsevier, pp. 271–XXXVI.
Roshan, S., DeVries, T., 2021. Global contrasts between oceanic cycling of cadmium and phosphate. Glob. Biogeochem. Cycles 35, e2021GB006952.
Roshan, S., Wu, J., 2015a. The distribution of dissolved copper in the tropical-subtropical North Atlantic across the GEOTRACES GA03 transect. Mar. Chem. 176, 189–198.
Roshan, S., Wu, J., 2015b. Cadmium regeneration within the North Atlantic. Glob. Biogeochem. Cycles 29, 2082–2094.
Roshan, S., Wu, J., 2015c. Water mass mixing: The dominant control on the zinc distribution in the North Atlantic Ocean. Glob. Biogeochem. Cycles 29, 1060–1074.
Roshan, S., DeVries, T., Wu, J., Chen, G., 2018. The internal cycling of zinc in the ocean. Glob. Biogeochem. Cycles 32, 1833–1849.
Rudnick, R.L., Gao, S., 2003. Composition of the continental crust. In: The Crust. Elsevier-Pergamon, Oxford.
Sarmiento, J.L., Gruber, N., Brzezinski, M.A., Dunne, J.P., 2004. High-latitude controls of thermocline nutrients and low latitude biological productivity. Nature 427, 56–60.
Schlitzer, R., Anderson, R.F., Dodas, E.M., Lohan, M., Geibert, W., Tagliabue, A., Bowie, A., Jeandel, C., Maldonado, M.T., Landing, W.M., 2018. The GEOTRACES intermediate data product 2017. Chem. Geol. 493, 210–223.
Schlitzer, R., 2021. Ocean Data View, odv.awi.de.
Schlosser, C., Karstensen, J., Woodward, E.M.S., 2019. Distribution of dissolved and leachable particulate Pb in the water column along the GEOTRACES section GA10 in the South Atlantic. Deep Sea Res. Part Oceanogr. Res. Pap. 148, 132–142.
Sloyan, B.M., Rintoul, S.R., 2001. Circulation, renewal, and modification of Antarctic mode and intermediate water. J. Phys. Oceanogr. 31, 1005–1030.
Solodoch, A., Stewart, A.L., Hogg, A.M., Morrison, A.K., Kiss, A.E., Thompson, A.F., Purkey, S.G., Cimoli, L., 2022. How does Antarctic bottom water cross the Southern Ocean? Geophys. Res. Lett. 49, e2021GL097211.
Stramma, L., England, M., 1999. On the water masses and mean circulation of the South Atlantic Ocean. J. Geophys. Res. Oceans 104, 20863–20883.
Stramma, L., Peterson, R.G., 1990. The South Atlantic current. J. Phys. Oceanogr. 20, 846–859.
Sunda, W.G., Huntsman, S.A., 2000. Effect of Zn, Mn, and Fe on Cd accumulation in phytoplankton: Implications for oceanic Cd cycling. Limnol. Oceanogr. 45, 1501–1516.
Sunda, W.G., 1975. The relationship between cupric ion activity and the toxicity of copper to phytoplankton (PhD Thesis). Massachusetts Institute of Technology.
Talley, L.D., 2011. Descriptive physical oceanography: an introduction. Academic press.
Tomczak, M., Large, D.G.B., 1989. Optimum multiparameter analysis of mixing in the thermocline of the eastern Indian Ocean. J. Geophys. Res. Oceans 94, 16141–16149.
Tortell, P.D., Rau, G.H., Morel, F.M.M., 2000. Inorganic carbon acquisition in coastal Pacific phytoplankton communities. Limnol. Oceanogr. 45, 1485–1500.
Twining, B.S., Baines, S.B., 2013. The trace metal composition of marine phytoplankton. Annu. Rev. Mar. Sci. 5, 191–215.
Twining, B.S., Baines, S.B., Vogt, S., Nelson, D.M., 2012. Role of diatoms in nickel biogeochemistry in the ocean. Glob. Biogeochem. Cycles 26, GB4001.
Twining, B.S., Rauschenberg, S., Morton, P.L., Vogt, S., 2015. Metal contents of phytoplankton and labile particulate material in the North Atlantic Ocean. Prog. Oceanogr. 137, 261–283.
van Aken, H.M., 2000. The hydrography of the mid-latitude Northeast Atlantic Ocean: I: the deep water masses. Deep Sea Res. Part Oceanogr. Res. Pap. 47, 757–788.
Vance, D., Little, S.H., de Souza, G.F., Khatiwala, S., Lohan, M.C., Middag, R., 2017. Silicon and zinc biogeochemical cycles coupled through the Southern Ocean. Nat. Geosci. 10, 202–206.

Wickham, H., Averick, M., Bryan, J., Chang, W., McGowan, L.D., François, R., Grolemund, G., Hayes, A., Henry, L., Hester, J., Kuhn, M., Pedersen, T.L., Miller, E., Bache, S.M., Müller, K., Ooms, J., Robinson, D., Seidel, D.P., Spinu, V., Takahashi, K., Vaughan, D., Wilke, C., Woo, K., Yutani, H., 2019. Welcome to the tidyverse. J. Open Source Softw. 4, 1686.

Woodward, E.M.S., Rees, A.P., 2001. Nutrient distributions in an anticyclonic eddy in the Northeast Atlantic Ocean, with reference to nanomolar ammonium concentrations. Deep Sea Res. Part II Top. Stud. Oceanogr. 48, 775–793.

Wyatt, N.J., Milne, A., Woodward, E.M.S., Rees, A.P., Browning, T.J., Bouman, H.A., Worsfold, P.J., Lohan, M.C., 2014. Biogeochemical cycling of dissolved zinc along the GEOTRACES South Atlantic transect GA10 at 40°S. Glob. Biogeochem. Cycles 28, 44–56.

Wyatt, N.J., Milne, A., Achterberg, E.P., Browning, T.J., Bouman, H.A., Woodward, E.M.S., Lohan, M.C., 2021. Seasonal cycling of zinc and cobalt in the South-Eastern Atlantic along the GEOTRACES GA10 section. Biogeosciences 18, 4265–4280.

Xie, R.C., Galer, S.J.G., Abouchami, W., Rijkenberg, M.J.A., De Jong, J., de Baar, H.J.W., Andreae, M.O., 2015. The cadmium–phosphate relationship in the western South Atlantic — The importance of mode and intermediate waters on the global systematics. Mar. Chem. 177, 110–123.

Živković, I., Humphreys, M.P., Achterberg, E.P., Dumousseaud, C., Woodward, E.M.S., Bojanić, N., Šolić, M., Bratkič, A., Kotnik, J., Vahčič, M., Obu Vazner, K., Begu, E., Fajon, V., Shlyapnikov, Y., Horvat, M., 2022. Enhanced mercury reduction in the South Atlantic Ocean during carbon remineralization. Mar. Pollut. Bull. 178, 113644.